Pak. J. Chem. 16(4): 161-186, 2026 Review article
ISSN (Print): 2220-2625
ISSN (Online): 2222-307X DOI: 10.15228/2026.v16.i4.p17

A review on Intelligent Manufacturing of Two-Dimensional Materials: From Batch Exfoliation to Automated, In-Line, and Continuous-Flow Production

Aoun Muhammad
Department of Chemistry, School of Natural Sciences(SNS), National University of Sciences and Technology (NUST), H-12, Islamabad, 44000, Pakistan
Corresponding Author email: aounm6886@gmail.com

Abstract
Two-dimensional (2D) nanomaterials, including graphene, hexagonal boron nitride (h-BN), transition-metal dichalcogenides (TMDs), and MXenes, possess unique electronic, mechanical, and surface properties that make them promising for electronics, energy storage, catalysis, and sensing. However, the industrial translation of exfoliation technologies remains limited because existing methods have rarely been assessed using consistent manufacturing-readiness criteria. This review evaluates mechanical, hydrothermal, electrochemical, and laser-assisted exfoliation methods based on production rate, yield, quality uniformity, reproducibility, cost, and tunability. Among the approaches reviewed, PEI-assisted sticky ball milling achieved over 40 g per batch with 97.9% monolayer content, while dual-electrode and alternating-current electrochemical exfoliation exceeded 25 $g.h^{-1}$ for graphene. Intermediate-assisted grinding exfoliation (iMAGE) demonstrated a favorable cost performance balance, achieving 67% h-BN yield at an energy consumption of 3.01×10^6 $J.g^{-1}$ using low-cost feedstocks. Emerging technologies such as machine learning, automated quality classification, in-line monitoring, and continuous-flow processing could further accelerate scale-up; robotic Bayesian optimization reduced experimental trials by approximately 21-fold, while GPU-based optical classification achieved about 95% pixel-level accuracy for flake thickness and coverage. However, no reported system has yet achieved fully closed-loop AI-controlled exfoliation, and most processes remain batch-based. Reliable industrial production will therefore require standardized cross-laboratory data, improved reactor and process control, continuous-flow systems, real-time quality monitoring, automation, and comprehensive techno-economic assessment.
Keywords: 2D materials, exfoliation, graphene; h-BN, TMDs

1. Introduction

The term exfoliation originates in geology and derives from the Latin word “folium”, meaning leaf. In its original context, it refers to the natural separation of thin, leaf-like layers from a bulk material, resembling the gradual peeling of an onion. Materials science has adopted this concept to describe a fundamental fabrication process in which atomically thin sheets, commonly known as two-dimensional (2D) materials, are isolated from their corresponding layered bulk crystals [1]. Since graphene was first isolated [2], the family of two-dimensional (2D) materials[3] has expanded considerably. Among the more recent additions are MXenes, a class of 2D transition-metal carbides, nitrides, and carbonitrides that has attracted substantial scientific and industrial attention. Their growing prominence arises from a distinctive combination of high stability, excellent mechanical strength, metallic electrical conductivity, and strong ion-adsorption capacity. Because of these properties, MXenes are promising materials for advanced applications, including high-strength composites, next-generation batteries, supercapacitors, and electromagnetic shielding [4, 5]. Graphene, first isolated in 2004, remains both the oldest and the most extensively studied 2D nanomaterial [6]. Ultrathin 2D nanomaterials exhibit distinctive advantages over other material forms. Their atomically thin, sheet-like architectures restrict electron motion to two dimensions, resulting in exceptional electronic properties that are highly valuable for advanced electronic technologies. The reduced thickness also imparts remarkable mechanical flexibility and optical transparency, enabling bendable, transparent devices. Equally important is their high surface-area-to-volume ratio, which enhances their performance in surface-dependent applications such as catalysis, sensing, and energy storage [7]. A major challenge for experimental researchers is achieving controlled, reproducible fabrication of 2D materials. Beyond the graphene family, which includes reduced graphene oxide, hexagonal boron nitride [h-BN], and g-C_3N_4, several other categories of 2D materials have been obtained. These include elemental 2D materials, also referred to as monoelemental nanosheets, such as silicene and phosphorene;[8] MXenes, comprising metal carbides, nitrides, and carbonitrides, with Ti_3C_2 and Mo_2N as representative examples; metal chalcogenides [9], including sulfides, selenides, and tellurides such as MoS_2 and $NiTe_2$; [10] 2D metal-organic frameworks (MOFs); covalent-organic frameworks (COFs);[11] and related material classes. Their laboratory-scale fabrication generally follows two principal routes: bottom-up and top-down methods. In the bottom-up strategy, materials are constructed directly from precursor atoms through techniques such as chemical or physical vapor deposition, atomic layer or molecular beam epitaxy, and hydrothermal synthesis. Although these methods typically yield high-quality products, the quantities produced are generally limited [12]. The biomaterials community widely recognizes that proteins adsorb rapidly under in vivo conditions and that this phenomenon plays a central role in determining the biological response to implanted materials [13]. Graphene was rapidly adopted in tissue-engineering research because of its exceptional mechanical strength, electrical and thermal conductivity, and biocompatibility[14]. In contrast, Layered Double Hydroxides (LDHs) have received comparatively limited attention relative to other families of 2D nanomaterials,

despite their considerable potential in biomedical engineering [15] LDH nanoparticles are increasingly being investigated as drug-delivery platforms because of their low toxicity and their capacity to bind anionic drug molecules and genetic material through noncovalent interactions [16]. LDH-based nanocomposites also demonstrate favorable mechanical and thermal characteristics compared with conventional polymeric scaffolds. For instance, incorporating LDH nanoparticles into a polymeric sheet can improve its mechanical stiffness[17]. Additional advantages of LDHs include high cytocompatibility, elevated charge density, anion-exchange capability, and pH-responsive drug-release behavior [17].

1.1. Scope, Comparability, and Limitations of this Review

Before presenting the manufacturing-readiness framework used throughout this review, three limitations of the underlying evidence base must be acknowledged. First, the comparisons drawn between exfoliation techniques in this review are not fully equitable. Production rate, exfoliation yield, monolayer content, and energy consumption are frequently reported under different experimental conditions, different feedstock quality, and different operational definitions of "yield" or "production rate." Direct ranking of techniques based on these figures alone should therefore be interpreted with caution; a rigorous cross-method comparison would require standardized multi-laboratory datasets, comparable feedstock quality, and a gap discussion.

Second, the literature surveyed in this review is weighted more heavily toward graphene and h-BN than toward other technologically important 2D materials, particularly transition-metal dichalcogenides (TMDs) and MXenes. This imbalance reflects the current state of the published scale-up literature rather than a deliberate editorial choice. Still, it does limit how broadly the conclusions of this review can be generalized across the full family of 2D materials. Where TMD- and MXene-specific scale-up data exist, they have been included, but readers should treat conclusions drawn primarily from graphene and h-BN studies as provisional when extrapolating to other material classes.

Third, production scale alone does not establish manufacturing readiness. A technique that produces large quantities of material is not necessarily industrially viable if it cannot also control flake size distribution, defect density, oxidation, contamination, solvent recovery, waste generation, and downstream purification. These parameters are addressed throughout and revisited critically, and they should be regarded as important to manufacturing readiness as raw production rate or batch size.

Future work in this area should prioritize integrating continuous-flow exfoliation, in-line characterization, and automated process control into single production platforms, rather than treating each as an isolated laboratory demonstration. In particular, coupling continuous-flow reactors with real-time Raman, optical, or NMR monitoring and closed-loop machine-learning control represents the most direct path toward determining whether high-performing laboratory exfoliation methods can be translated into genuinely sustainable, industrial-scale production.

Realizing this translation will additionally require a standardized techno-economic and life-cycle assessment (TEA/LCA) framework, supported by independent multi-laboratory validation, so that claims of scalability can be benchmarked on a common basis rather than compared informally across heterogeneous studies. Such a framework should explicitly capture environmental and economic metrics that are rarely reported in the exfoliation literature, including solvent use and recovery, energy intensity per gram of product, waste generation, and reagent recyclability, alongside the production-rate and yield metrics that dominate current reporting. These metrics are revisited quantitatively, where data allow.

Table 1. Classification of major 2D material families reviewed, with representative members, structural features, and applications.

Material class	Representative members	Key structural/compositional features	Example applications	Ref
Graphene family	Graphene, rGO, h-BN, g-C_3N_4	Atomically thin, sp^2-bonded sheets; high conductivity & flexibility	Flexible electronics, tissue engineering	[6, 7] [14]
Elemental (monoelemental)	Silicene, phosphorene	Single-element 2D lattices	Emerging electronic/optoelectronic devices	[8]
MXenes	Ti_3C_2, Mo_2N	Transition-metal carbides/nitrides/carbonitrides; metallic conductivity, ion adsorption	Batteries, supercapacitors, EM shielding	[4, 5], [9]
Metal chalcogenides (TMDs)	MoS_2, $NiTe_2$	Sulfides/selenides/tellurides; tunable bandgap, phase polymorphism	Transistors, photodetectors, catalysis	[10]
2D MOFs / COFs	Molecularly intercalated MOFs, COF sheets	Porous, tunable organic -inorganic frameworks	Catalysis, sensing, gas storage	[11]
Layered double hydroxides (LDHs)	Mg/Al LDH	Anion exchange capacity, pH-responsive release	Drug delivery, biomedical composites	[15-17]

Abbreviations: rGO, reduced graphene oxide; h-BN, hexagonal boron nitride; g-C_3N_4, graphitic carbon nitride; TMDs, transition-metal dichalcogenides; MOF, metal–organic framework; COF, covalent-organic framework; LDH, layered double hydroxide.

1.2. Manufacturing-Readiness Criteria for Exfoliation Technologies

1.2.1. Production Rate

Production rate is a key indicator of scalability in the exfoliation of 2D materials, as it reflects whether a technique can progress from laboratory proof-of-concept to continuous and economically feasible manufacturing. Of the studies reviewed, PEI-assisted sticky ball milling achieved the highest batch-scale output, producing more than 40 g of graphene per batch while retaining a monolayer content of 97.9% and a yield of 78.3% [18] Intermediate-assisted grinding

exfoliation also exhibited notable production efficiency, generating 2D h-BN at a rate of 0.3 g h^{-1} with a 67% yield. In the same study, exfoliation of molybdenite-derived MoS_2 yielded 60 L of dispersion at a concentration of 0.25 mg mL^{-1} in less than 270 min, corresponding to approximately 15 g of exfoliated material [19] Additive-assisted shear exfoliation of WS_2, by comparison, produced 2.8 ± 0.4 g of nanoflakes within 90 min, equivalent to an estimated production rate of 1.87 g h^{-1}, while increasing exfoliation efficiency by more than 400% relative to conventional shear exfoliation [20]. Polymer-assisted dry ball milling of h-BN showed a substantially lower processing capacity under typical conditions, treating only 100 mg of h-BN over 2 h, which corresponds to an estimated feed-processing rate of 50 mg h^{-1}. However, the absence of data on actual recovered nanosheet yield prevents direct comparison with methods reporting higher outputs [21]. Taken together, these findings indicate that additive- and intermediate-assisted mechanical exfoliation strategies can markedly increase production rates compared with conventional sonication-based approaches. Nevertheless, meaningful cross-study evaluation of scalability remains constrained by inconsistent reporting of recovered mass, yield, and time-normalized production output.

1.2.2. Exfoliation Yield

Exfoliation yield describes the proportion of a bulk layered precursor that is successfully transformed into usable mono- or few-layer 2D nanosheets. It is a central measure of scalability because a high conversion yield must be obtained without compromising nanosheet quality, thickness uniformity, or lateral dimensions. The highest yield among the reviewed studies was achieved by Wang et al. (2023) [18], who used PEI-assisted sticky mechanical exfoliation to produce graphene from graphite with a 97.9% monolayer percentage and a 78.3% yield. Depending on the milling duration, the apparent graphene yield increased to as much as 90.7%. A similarly effective mechanical strategy was reported by [19] (Zhang et al. (2020), whose IMAGE technique generated pristine 2D h-BN with an exfoliation yield of 67%, substantially higher than the yields of below 3% commonly reported for conventional liquid-phase exfoliation. By comparison, [20] Nguyen et al. (2021) obtained a 30–31% yield of few-layer WS_2 through additive-assisted shear exfoliation. Lithium-intercalation approaches, as discussed by [22] (Chavalekvirat et al. (2024), can produce monolayer TMDs at yields exceeding 90%; however, their broader scalability is restricted by safety risks, phase transitions, and processing-related challenges. Collectively, these methods reveal a distinct trade-off between yield and nanosheet quality. Increasing milling duration, shear rate, sonication power, or additive concentration can enhance exfoliation yield or monolayer content but may simultaneously decrease lateral flake size, promote fragmentation, leave residual additives, or require further purification. An optimal exfoliation method should therefore not be selected solely on the basis of its numerical yield. Instead, it should provide high conversion efficiency and mono- or few-layer selectivity while preserving large lateral dimensions, minimizing defect formation, and remaining suitable for practical industrial-scale production [18-20, 22].

1.2.3. Quality Control

1.2.3.1. Characterization Methods (Raman, AFM)

Quality uniformity in exfoliated 2D materials describes the degree of consistency in layer number, flake thickness, lateral-size distribution, defect density, structural integrity, and interfacial cleanliness throughout a produced sample. This parameter is essential because reliable device performance depends not only on exfoliation yield but also on the reproducibility of nanosheet quality. The most favorable quality outcome was achieved through ultrahigh-vacuum exfoliation, in which ultraflat, contamination-free substrates facilitated the formation of monolayer or bilayer 2D materials with near-ideal interfaces. AFM and Raman analysis confirmed thickness, while adsorbates, bubbles, oxidation, and surface contamination were substantially reduced [23, 24] (Sun et al., 2022). Paton et al. (2023) demonstrated that mass-produced graphene nanoplatelets nevertheless retained considerable heterogeneity. AFM measurements revealed flake heights of 2.8–15.6 nm, with 85.3% of the flakes measuring below 10 nm, whereas lateral dimensions ranged from 85 to 385 nm. Raman mapping further indicated that classifying individual spectra provides a more reliable way to identify unexfoliated graphite than evaluating averaged spectra. By comparison, [25] (Gasbarro et al. (2025) developed a high-throughput optical-classification method capable of assessing flake coverage and layer thickness across extensive image datasets with approximately 95% pixel-wise accuracy. Although this approach is valuable for statistically evaluating thickness uniformity, it does not directly characterize defects through Raman, AFM, or TEM analysis. A persistent limitation is that samples appearing uniform may still contain thicker flakes, residual material, or unexfoliated particles. Averaged Raman spectra could not reliably identify graphite contents of up to 10 wt% and exhibited minimal variation even after substantial sediment addition. Optical techniques may likewise misclassify thick flakes and residues when their RGB contrast values overlap [24, 25]. Consequently, an appropriate quality standard for scalable 2D-material exfoliation should incorporate narrow, experimentally verified thickness distributions, consistent layer numbers across large areas, minimal contamination, and preservation of structural integrity. Such evaluation should rely on multimodal characterization, including Raman/AFM-assisted mapping or high-throughput optical classification, rather than averaged measurements alone.

1.2.3.2. Thickness & Layer Control

Thickness and layer-number uniformity are essential for reproducible properties and device performance of 2D materials. Fourier imaging micro-ellipsometry enables precise thickness mapping and identification of mono-, bi-, and trilayer

materials; for $MoSe_2$, monolayer and bilayer thicknesses of 0.603 ± 0.01 and 1.266 ± 0.04 nm, respectively, were reported [26, 27]. Exfoliation studies further demonstrate a correlation between thickness and lateral-size distribution, with thicker nanosheets generally associated with narrower size distributions, whereas thinner sheets may show greater lateral polydispersity [26]. UHV exfoliation provides another effective route to highly selective monolayer production, achieving bulk-crystal-sized MoS_2 monolayers with exfoliation efficiencies approaching 100% [28]. In CVD synthesis, controlling sulfur concentration influences the size, shape, uniformity, and crystal quality of monolayer MoS_2 [29]. Thus, scalable production requires simultaneous control of layer number, lateral dimensions, crystallinity, and surface quality, supported by complementary characterization techniques such as AFM, Raman spectroscopy, PL, and optical microscopy [26–29].

1.2.3.3. Defect Control & Structural Quality

Defects in 2D materials may arise as vacancies, edge damage, oxidation, residual contaminants, phase impurities, basal-plane disorder, or lattice distortions. Controlling these imperfections is crucial because they can substantially influence charge transport, optical behavior, chemical stability, and the reproducibility of device performance[30-33] . Among the methods reviewed, solvent-based liquid exfoliation of graphene provided the strongest evidence of low defect density. Raman spectra showed no D band in large flakes, while XPS revealed a spectrum dominated by C–C bonding with minimal oxidation, indicating the formation of defect- and oxide-free graphene [31]. Improved liquid-phase exfoliation of MoS_2/graphene heterostructures also preserved structural quality, as shown by weak graphene D-band intensity; low ID/IG values of 0.1680 for graphene and 0.2092 for MoS_2/graphene; retention of the semiconducting 2H phase of MoS_2; few-layer thickness confirmed by AFM; and hexagonal crystallinity verified by SAED [30]. Electrochemical exfoliation, by comparison, provides greater control over defect density, oxygen content, and crystal structure. However, anodic routes may promote oxidation, including 15.6 at% oxidized Mo in MoS_2. In contrast, cathodic approaches employing organic electrolytes or quaternary ammonium ions are more effective at preserving crystallinity and suppressing the undesirable 2H-to-1T phase transformation [32]. A major limitation common to scalable exfoliation techniques is balancing high yield with structural integrity. Extended sonication may increase Raman D-band signals associated with edge defects, electrochemical methods can induce oxidation or phase changes, and additive-assisted shear exfoliation requires post-filtration to eliminate PTFE residues while minimizing fragmentation at elevated shear rates [30-33] An ideal advanced exfoliation method should therefore produce few-layer or monolayer nanosheets at high yield while maintaining intact basal planes, low ID/IG ratios or other defect signatures, preserved phase purity, minimal oxidation, and freedom from residual contaminants. These characteristics should be confirmed through complementary Raman, XPS, AFM, TEM/SAED, and optical characterization. [30-33].

1.2.4. Defect Density and Structural Integrity at Scale

Defects in 2D materials, including vacancies, basal-plane damage, edge disorder, oxidation, surface contamination, lattice strain, phase impurities, and interfacial trap states, strongly govern carrier mobility, optical response, thermal transport, chemical stability, and the reproducibility of large-area devices [34-37]. Among the reviewed approaches, modified mechanical exfoliation provided the strongest evidence of structural preservation. Large-area graphene exhibited an exceptionally weak Raman D band at ~1350 cm^{-1}, with its intensity remaining below 0.4% of the 2D peak. AFM further confirmed smooth and uniform flakes with no obvious structural damage. At the same time, the resulting devices achieved mobilities of ~4000 $cm^2 V^{-1} s^{-1}$ under back-gating and ~12,000 $cm^2 V^{-1} s^{-1}$ under solution top-gating [35, 36].
Similarly, ultrasonic exfoliation in liquid nitrogen (UEILN) effectively minimized structural degradation in h-BN. SEM and TEM revealed no evident surface damage, HRTEM confirmed highly crystalline basal planes, and SAED showed well-defined hexagonal diffraction patterns. XPS and FTIR also indicated fewer defect-associated B–O and B–OH species than conventional ultrasonic exfoliation in organic solvents [34]. In contrast, solvent-based ultrasonic exfoliation can induce cavitation-driven surface damage and oxidation. UEILN mitigates intralayer damage by maintaining a more favorable balance between expansion and bond-breaking energies [34]. For defect-sensitive 2D metal oxides, structural integrity additionally depends on controlling oxygen vacancies, stoichiometry, phase purity, interfacial contamination, and lattice strain [34-37]. A major unresolved challenge is the yield-quality trade-off in scalable exfoliation. Increasing exfoliation energy or processing intensity may improve throughput but simultaneously promotes fragmentation, vacancy generation, oxidation, surface contamination, phase instability, and defect-induced charge scattering [34-37]. Thus, scalability should not be evaluated solely by nanosheet yield; it must also be assessed against quantitative structural and functional quality metrics. An effective large-scale strategy should produce large-area, few-layer nanosheets with intact basal planes, low Raman defect signatures, preserved crystallinity, controlled vacancy concentrations, minimal oxidation, clean interfaces, stable phases, and reproducible electrical performance, supported by complementary Raman, AFM, TEM/HRTEM, SAED, XPS, and electrical characterization [34-37].

1.2.5. Reproducibility

Reproducibility in scalable 2D-material production describes the capacity of an exfoliation or synthesis method to produce nanosheets with comparable thickness, lateral dimensions, morphology, and overall quality across repeated experiments, different operators, and separate manufacturing batches. This consistency is a fundamental requirement for industrial implementation. Among the reviewed approaches, polymer-assisted dry ball-milling appears to offer the greatest reproducibility potential because it replaces manually controlled tape exfoliation with an automated process

governed by defined operating parameters. In starch-assisted milling, the hBN thickness distribution shifted from approximately 10–200 nm in conventional dry ball-milling to predominantly 10–20 nm, and the principal thickness peak shifted from about 25 nm to 7 nm [21]. Wider industrial assessments similarly identify reproducibility, batch-to-batch consistency, and large-area uniformity as essential manufacturing criteria, whereas liquid exfoliation and wet chemical synthesis remain constrained by low yield, non-uniform nanosheet thickness, size heterogeneity, and defect-associated instability [38]. Reproducibility can be adversely affected by operator-dependent tape exfoliation, inadequately quantified pressure during manual peeling, uncontrolled tape-removal speed and angle, folding and contamination introduced during CVD transfer, and limited control of layer number in wafer-scale synthesis [21, 25, 38]. Automation and process standardization are therefore emerging as important solutions. Examples include machine-learning-guided polymer selection for ball-milling and GPU-accelerated optical classification, which achieved approximately 95% pixel-wise accuracy while analyzing 2916 images in about 35 min to enable high-throughput comparison of exfoliation trials [21, 25]. Reproducibility should consequently be regarded not only as a reporting parameter but also as a critical process-control requirement for transforming advanced exfoliation strategies into dependable, scalable, and application-specific industrial production routes for 2D materials.

1.2.6. Cost and Energy Demand

Cost is a critical consideration in the scalable production of 2D materials, encompassing not only reagent expenses but also energy demand, processing duration, equipment requirements, solvent management, post-treatment, and the overall feasibility of manufacturing gram-to-ton-scale quantities without compromising flake quality. Among the methods reviewed, intermediate-assisted grinding exfoliation appears to provide the most favorable balance between cost and performance because Zhang et al. [19] achieved a 67% exfoliation yield, a production rate of 0.3 g h^{-1}, and a low energy consumption of 3.01×10^6 J g^{-1} for h-BN. The method also employed inexpensive intermediates, including sea sand, and demonstrated MoS_2 production from low-cost natural molybdenite concentrate. Polymer-assisted dry ball milling represents another economically promising strategy, as Zhang et al.s][21] converted a conventional industrial powder-processing technique into an automated exfoliation route by using inexpensive natural polymers such as starch and gelatin. This approach reduces dependence on costly or harsh chemical treatments while retaining the potential for scalable operation. Liquid-phase exfoliation, by contrast, is potentially cost-effective because it can produce large quantities of solution-based materials; however, its actual economic burden depends heavily on sonication time, acoustic power, solvent selection, surfactant concentration, centrifugation, and surfactant-removal procedures. Sonication may continue for several hours to hundreds of hours, increasing energy consumption, while organic solvents such as NMP and DMF add toxicity, handling, and solvent-removal costs[22]. Bottom-up approaches, including processable 2D CVD and PVD, are generally less economical for bulk production because high-temperature growth, vacuum operation, slow deposition rates, and transfer procedures increase operating expenses and limit production output [19, 22] . Overall, the available evidence indicates that mechanical methods based on inexpensive solid additives or natural feedstocks, particularly iMAGE and polymer-assisted dry ball milling, are more industrially realistic than solvent-intensive or high-vacuum techniques. Nevertheless, none of the reviewed studies reported a complete cost-per-gram assessment, preventing a definitive economic comparison among the available methods [19].

1.2.7. Tunability

Tunability in 2D-material production refers to the ability to control layer number, thickness, flake size, phase structure, bandgap, surface chemistry, and application-specific properties. This is critical because 2D-material performance strongly depends on its structural and dimensional characteristics. Among the reviewed methods, liquid-phase exfoliation offers the greatest tunability, as sonication, solvent and surfactant conditions, centrifugation, and electrochemical potential can regulate flake size, thickness, monolayer yield, surface charge, bandgap, and phase transitions in TMDs such as MoS_2 [22]. Polymer-assisted dry ball milling also controls nanosheet morphology, with polymer properties and processing conditions influencing the thickness, lateral size, and aspect ratio of hBN nanosheets; starch-assisted milling can produce ultrathin, high-aspect-ratio flakes suitable for printing and coatings [21]. Whereas mechanical exfoliation enables scalable control of thickness, flake size, and structural integrity but offers limited control over bandgap, doping, functionalization, and phase engineering [19]. Thus, liquid-phase and electrochemical methods are preferable when precise electronic, optical, or electrochemical properties are required. In contrast, dry mechanical methods are advantageous for scalable production with controlled thickness, flake size, and morphology [19,21,22].

1.3. Force-Driven Exfoliation

1.3.1. Driving Force and Working Mechanism

Mechanical exfoliation is the earliest and remains one of the most dependable top-down strategies for producing high-quality two-dimensional (2D) materials. It operates by applying external forces sufficient to overcome the weak van der Waals interactions that hold adjacent layers together in bulk layered crystals. The method gained global prominence following the isolation of monolayer graphene from graphite with adhesive tape, an achievement that laid the groundwork for modern research on 2D materials [39]. Although conventional Scotch-tape exfoliation can generate atomically thin nanosheets with nearly pristine crystalline quality, its manual and sequential layer-peeling process severely limits scalability. [40, 41]. Efforts to address these limitations have led to the development of numerous advanced mechanical

techniques, including viscoelastic-stamp exfoliation, Au-, Ag-, oxygen plasma-, and Al_2O_3-assisted exfoliation, rheometer-assisted automated exfoliation, shear exfoliation, ball milling, intermediate-assisted grinding exfoliation (iMAGE), and polymer-assisted ball milling [19, 21, 41, 42]. Across these approaches, applied shear, compression, or impact forces induce interlayer displacement and nanosheet separation. Solvents, surfactants, and engineered surface interactions may also prevent restacking and enhance exfoliation efficiency. More recent investigations have shown that both substrate–material interactions and machine-learning-assisted optimization are important for regulating exfoliation behavior and the resulting nanosheet morphology [26, 41].

1.3.2. Scale-Up Evidence and Benchmark Performance

Among top-down techniques, mechanical exfoliation consistently produces 2D materials of the highest structural quality. Conventional adhesive-tape methods routinely generate defect-free monolayer graphene, few-layer black phosphorus, AlN nanosheets, graphene electrodes, and various transition metal dichalcogenides (TMDs). Their excellent crystallinity has been verified using AFM, Raman spectroscopy, TEM, STM, PL, and electrical transport measurements. [2, 40, 41, 43-45]

Recent scalable variants have achieved substantial productivity improvements. High-shear exfoliation, for instance, reached a production rate of 1.44 g h^{-1}, whereas kitchen-blender exfoliation produced material at 0.15 g h^{-1}. Intermediate-assisted grinding exfoliation (iMAGE) achieved a 67% exfoliation yield and a production rate of 0.3 g h^{-1}, producing nanosheets with an average thickness of 4 nm and lateral dimensions of approximately 1.2 μm. The process also exhibited a notably low energy consumption of 3.01×10^6 J g^{-1} $^{-1}$ [19]. Ball milling has likewise shown high efficiency, with optimized MoS_2 exfoliation reaching yields of up to 95%. Polymer-assisted dry ball milling further improved the process through mechanical gripping and machine-learning-guided optimization [21, 39]. Au-assisted exfoliation represents another major advance, delivering nearly 100% monolayer preparation efficiency and enabling the production of millimeter- to centimeter-scale monolayers [41]. The primary strength of mechanical exfoliation lies in its ability to retain the intrinsic crystalline structure of layered materials while introducing minimal defects and chemical contamination. Mechanically exfoliated nanosheets therefore continue to serve as reference materials for examining the intrinsic electrical, optical, magnetic, and quantum properties of 2D systems [40, 41] . The method is also highly versatile and has been successfully applied to graphene, h-BN, MoS_2, WS_2, WSe_2, $MoSe_2$, $MoTe_2$, black phosphorus, AlN, Bi_2Te_3, metal oxides, MXenes, and many other layered compounds [19, 39]

Several recent developments have improved process control and reproducibility. Rheometer-assisted exfoliation enables automated operation under precisely regulated normal and shear forces, while viscoelastic polymer stamps reduce contamination relative to conventional adhesive tapes [46, 47]. Intermediate-assisted grinding and polymer-assisted ball milling offer additional scalability advantages by combining high exfoliation yields and low energy requirements with compatibility with established industrial equipment [19, 21]. Together, these advances have reduced the divide between laboratory-scale preparation and industrial manufacturing without sacrificing the exceptional material quality associated with mechanical exfoliation.

1.3.3. Quality Risks and Failure Mechanisms

Despite producing materials of outstanding quality, mechanical exfoliation still presents important obstacles to large-scale industrial adoption. Traditional tape-assisted methods are labor-intensive, generate relatively small flakes, provide low throughput, and are poorly suited to industrial production requirements [39, 40]. Scalable mechanical techniques also introduce their own limitations. Shear exfoliation often has comparatively low exfoliation efficiency and may require additional processing, such as cascade centrifugation, to remove unexfoliated material, thereby increasing overall production costs [39]. Prolonged ball milling can cause excessive intralayer fracture, reducing lateral flake dimensions and making careful control of milling speed, ball size, surfactant concentration, and processing time essential [39]. Material-specific instability presents a further difficulty. Mechanically exfoliated black phosphorus, for example, degrades rapidly under ambient conditions because of its environmental instability [44]. Major unresolved priorities therefore include achieving consistent layer numbers, precise thickness regulation, reproducibility between laboratories, and economically feasible production of large-area nanosheets [41].

1.3.4. Process Intensification and Automation

Mechanical exfoliation has evolved considerably from a simple manual laboratory procedure into a broad group of increasingly scalable manufacturing strategies. Surface-assisted techniques based on Au, Ag, oxygen plasma, and Al_2O_3 enhance interfacial interactions and substantially improve exfoliation efficiency, allowing large-area monolayers to be produced without compromising crystal quality [41]. Rheometer-assisted automation accurately regulates normal and shear forces, reducing operator dependence and improving experimental reproducibility [46].

In intermediate-assisted grinding exfoliation, hard microparticles transform applied compressive forces into localized microscopic shear forces, enabling high-yield exfoliation with lower energy consumption [19]. Polymer-assisted dry ball milling similarly uses mechanical gripping, combined with machine-learning-based optimization, to enhance exfoliation efficiency and strengthen process control [19, 21]. Machine-learning-guided optimization has also been used to selectively regulate nanosheet thickness by establishing relationships between thickness and lateral-size distributions. At the same time, advanced Raman-based evaluation has improved detection of residual unexfoliated graphite in

mechanically processed graphene samples [24, 26]. Collectively, these developments reflect a broader shift from empirically controlled exfoliation toward intelligent, standardized, reproducible, and industrially relevant manufacturing.

Table 2. Comparative scale-up metrics for force-driven (mechanical) exfoliation: production rate, yield, dimensions, and quality.

Method	Production rate	Yield	Thickness / lateral size	Energy/time	Quality notes	Ref
PEI-assisted sticky ball milling (graphene)	>40 g/batch	78.3% (up to 90.7%)	Monolayer 97.9%	—	—	[18]
Intermediate-assisted grinding, iMAGE (h-BN)	0.3 g h^{-1}	67%	4 nm thick, 1.2 μm lateral	3.01×10^{6} $J.g^{-1}$	vs <3% for conventional LPE	[19]
iMAGE (MoS_2 from molybdenite)	~15 g in <270 min (60 L @ 0.25 mg mL^{-1})	—	—	—	Low-cost natural feedstock	[19]
Additive-assisted shear (WS_2)	1.87 g h^{-1} (2.8±0.4 g/90 min)	30–31%	—	—	+400% efficiency vs conventional shear	[20]
Polymer-assisted dry ball milling (h-BN)	50 mg h^{-1} (feed)	Not reported	Thickness peak shifted 25→7 nm	—	ML-guided polymer selection	[21]
High-shear exfoliation (general)	1.44 g h^{-1}	—	—	—	—	[39]
Kitchen-blender exfoliation	0.15 g h^{-1}	—	—	—	—	[39]
Au-assisted exfoliation	—	~100% monolayer efficiency	mm–cm scale monolayers	—	Near-pristine crystallinity	[41]
Optimized ball milling (MoS_2)	—	up to 95%	—	—	—	[21, 39]

Abbreviations: PEI, polyethyleneimine; iMAGE, intermediate-assisted grinding exfoliation; LPE, liquid-phase exfoliation; ML, machine learning. Em dash (—) indicates value not reported in the cited source.

1.4. Thermochemical Exfoliation

1.4.1. Driving Force and Mechanism

Hydrothermal exfoliation is a top-down processing route in which a layered bulk material is dispersed in a reaction medium and subjected to combined thermal, chemical, and pressure effects within a sealed autoclave. These conditions weaken interlayer interactions and facilitate the separation of bulk materials into nanosheets [39]. The process generally proceeds through two main pathways: intercalation-assisted and reaction- or etching-assisted exfoliation. In intercalation-assisted exfoliation, ions, solvent molecules, or molecular spacers enter the interlayer galleries under elevated temperature and autogenous pressure. Their insertion increases the interlayer spacing, promotes electrostatic repulsion, and reduces van der Waals interactions between adjacent layers. Various species, including Li^+, Na^+, Fe^{2+}, hydrazine-derived species, ammonium carbonate, and organic molecules, have been employed as intercalants, while water, isopropanol, ethanol, ethylene glycol, DMF, and aqueous–organic mixtures can serve as reaction media.

Reaction- or etching-assisted exfoliation involves selective chemical removal or bond cleavage that generates defects or reactive sites and facilitates subsequent delamination. Representative examples include molecular intercalation in metal–organic frameworks and chemical etching of MXene precursors. In many cases, hydrothermal treatment is followed by mechanical separation, such as stirring, ultrasonication, high-shear mixing, or centrifugation. For example, Li^+-assisted exfoliation of h-BN involves interlayer expansion through ion intercalation, followed by mechanical stirring, whereas ammonium-carbonate-treated MoS_2 undergoes partial expansion during hydrothermal treatment before high-speed shearing produces few-layer nanosheets [48,49].

1.4.2. Scale-Up Evidence and Benchmark Performance

The performance of hydrothermal exfoliation depends strongly on the starting material, solvent, intercalant, and whether mechanical treatment is used. Reported yields generally range from 10–50%, with nanosheet thicknesses below five layers and production rates exceeding 1 g h^{-1}; however, these values represent broad literature ranges rather than a standardized process. Wang et al. [48] reported a 55% yield for h-BN treated in isopropanol containing LiCl at 180 °C for 12 hr under approximately 2 MPa autogenous pressure with mechanical stirring. The resulting nanosheets had a concentration of 4.13 mg mL^{-1}, thicknesses of 0.5–2.8 nm, and lateral dimensions of up to approximately 10 μm. Sharma and Puri [50] prepared nearly 1 μm-wide few-layer h-BN using hydrazine hydrate in an IPA–water medium at 220 °C for 18 h. Although the gravimetric exfoliation yield was not reported, the optimized material showed a crystallite size of 1.15 nm, a 71.04% increase in electroactive area, and a 69.96% enhancement in redox current compared with bulk h-BN.

More recently, an alkali-hydrothermal-assisted shear process produced hydroxylated BNNS with a 65% yield and a concentration of 9.8 mg mL^{-1}. Treatment at 200 °C for 4 h, followed by 2 h of high-shear mixing, generated nanosheets with an average thickness of 2.54 nm and a lateral size of 1.41 μm [51]. For MoS_2, hydrothermal treatment with ammonium carbonate followed by shearing produced approximately 4–6 layers with AFM-measured thicknesses of 2.70–3.59 nm. A separate Na^+-intercalation-assisted solvothermal method produced MoS_2 quantum dots with a reported yield of 20%, a lateral size of 3.7 nm, and a thickness of 1.2 nm [49,52]. Across these studies, XRD, Raman, AFM, TEM, HRTEM, XPS, and FTIR analyses generally confirmed retention of the original crystalline phases, limited oxidation

under optimized conditions, reduced layer numbers, and preservation of lattice order. However, monolayer fractions remained relatively low, reaching only about 5% in the Li^+-assisted h-BN process.

A major advantage of hydrothermal exfoliation is its ability to combine interlayer weakening, nanosheet separation, surface modification, and dispersion stabilization within a single processing platform. Unlike prolonged sonication, which can cause progressive flake fragmentation, hydrothermal intercalation weakens the layered structure before mechanical separation, thereby facilitating delamination. For comparison, O'Neill et al.,[53] required approximately 140 h of probe sonication to obtain a 40% MoS_2 dispersion yield, with ultrasonic scission reducing flake lateral dimensions.

Hydrothermal processing can therefore preserve relatively large nanosheets while reducing their thickness. For example, following Li^+ intercalation, the lateral size of h-BN increased from approximately 0.4 to 10 μm, whereas the thickness decreased from approximately 3 to 2 nm [48]. The method also offers considerable chemical flexibility because solvent polarity, surface tension, cation size, pH, temperature, and reaction time can be adjusted to suit exfoliation requirements and the surface chemistry of different materials. Its demonstrated applicability to h-BN, graphite, graphene, MoS_2, WS_2, VO_2, α-MoO_3, metal–organic frameworks, MXenes, metal hydroxides, and emerging two-dimensional borides highlights its broad material scope. Hydrothermal processing can also introduce useful surface functionality in situ. Treatment with NaOH/KOH increased the h-BN interlayer distance from 3.32 to 3.45 Å and generated B–OH groups, substantially improving aqueous dispersibility and polymer compatibility [51]. Hybrid hydrothermal routes may further preserve the desired crystalline phase, such as semiconducting 2H-MoS_2, while minimizing the basal-plane damage and uncontrolled functionalization associated with aggressive ball milling or oxidation-based exfoliation.

1.4.3. Quality Risks and Failure Mechanisms

Despite its potential benefits, hydrothermal exfoliation involves elevated temperatures, pressure-resistant reactors, prolonged residence times, and extensive downstream processing. Reported treatments commonly operate at 150–250 °C for 2–18 h, while some intercalation or chemical-conversion routes require ≥24 h. Cooling, washing, centrifugation, dialysis, filtration, and drying further increase processing time and energy demand. Sealed-autoclave operation also introduces safety, corrosion, heat-transfer, and scale-up challenges, while reaction pressure is often reported only as "autogenous" without direct measurement [39].

Product uniformity is another limitation. Incomplete intercalation can yield mixtures of unexfoliated particles, multilayers, and few-layer nanosheets, often requiring additional size-selection steps that reduce recovery. Residual Li^+, Na^+, hydrazine, strong alkalis, fluoride-based etchants, or high-boiling solvents may contaminate the product and alter its electronic properties. HF-based MXene processing is particularly concerning because of its handling and environmental hazards [39].

Moreover, hydrothermal treatment alone may not achieve complete exfoliation, and ultrasonication or high-speed shearing is often required. This complicates attribution of yield and product quality solely to the hydrothermal step. In some cases, mechanical approaches offer simpler and potentially higher-throughput alternatives; for example, intermediate-assisted grinding produced h-BN at 0.3 g h^{-1} with 67% yield, while PTFE-assisted shear exfoliation achieved approximately 31% WS_2 yield within 90 min without autoclave heating. Thus, hydrothermal methods should be justified by demonstrable advantages in material quality, functionality, or versatility that outweigh their thermal, chemical, and processing complexity [19,33]. Table 3 tabulates comparative scale-up metrics for thermochemical exfoliation production rate, yield, dimensions, energy, and quality.

Table 3. Comparative scale-up metrics for thermochemical exfoliation production rate, yield, dimensions, energy, and quality.

Method	Production rate	Yield	Thickness / lateral size	Energy/time	Quality notes	Ref
Li^+-intercalation h-BN (LiCl/IPA, 180 °C, 12 h, ~2 MPa)	—	55%	0.5–2.8 nm thick, ~10 μm lateral	4.13 mg mL^{-1} conc.	—	[48]
Hydrazine-assisted h-BN (IPA–water, 220 °C, 18 h)	—	Not reported	Crystallite 1.15 nm	—	+71.04% electroactive area, +69.96% redox current	[50]
Alkali (NaOH/KOH) hydrothermal–shear BNNS	—	65%	2.54 nm thick, 1.41 μm lateral	200 °C/4 h + 2 h shear	Composite thermal conductivity 7.58 W $m^{-1}K^{-1}$	[51]
Ammonium-carbonate MoS_2 (hydrothermal + shear)	—	—	2.70–3.59 nm (4–6 layers)	—	—	[49, 52]
Na^+-intercalation solvothermal MoS_2 quantum dots	—	20%	1.2 nm thick, 3.7 nm lateral	—	—	[49, 52]
Probe sonication MoS_2 (benchmark comparison)	—	40%	Lateral size reduced by scission	140 h	—	[53]
Ammonium-carbonate MoS_2 (hydrothermal + shear)	—	—	2.70–3.59 nm (4–6 layers)	—	—	[49, 52]
Na^+-intercalation solvothermal MoS_2 quantum dots	—	20%	1.2 nm thick, 3.7 nm lateral	—	—	[49, 52]

Abbreviations: Li^+, lithium ion; h-BN, hexagonal boron nitride; LiCl, lithium chloride; IPA, isopropyl alcohol; NaOH, sodium hydroxide; KOH, potassium hydroxide; BNNS, boron nitride nanosheets; MoS_2, molybdenum disulfide; Na^+, sodium ion.

Units: °C, degrees Celsius; MPa, megapascal; mg mL^{-1}, milligrams per milliliter; nm, nanometer; µm, micrometer; W m^{-1} K^{-1}, watts per meter-kelvin; h, hour.

1.4.4. Recent Innovations and Improvements

Recent advances have transformed hydrothermal exfoliation from a simple heated-intercalation method into a multifunctional processing platform. Solvent engineering has improved exfoliation efficiency; for example, IPA outperformed DMF, NMP, 1-octanol, and water in Li^+-assisted h-BN exfoliation because its surface tension better matched the modified surface energy of the intercalated material. Hydrazine-assisted IPA water processing enabled simultaneous exfoliation and redox functionalization, while NaOH treatment in ethanol followed by DMF sonication produced ultrasmall MoS_2 quantum dots with improved yield [50,52].

Mechanical intensification has further enhanced exfoliation. Ammonium carbonate-assisted hydrothermal expansion followed by rotary-blade shearing produced 4–6-layer MoS_2. In contrast, mixed NaOH/KOH treatment combined with high-shear processing yielded hydroxylated BNNS at 65%, with an exfoliation efficiency of 32.5% h^{-1}. Other approaches include ultrasonic–hydrothermal treatment for ~1.48 nm-thick α-MoO_3 monolayers, mixed Li^+/Na^+ intercalation for faster graphite delamination and improved colloidal stability, and molecular-intercalation reactions producing ~1 nm-thick MOF nanosheets with a 57% yield [36,39].

Microwave-hydrothermal processing has reduced reaction times to approximately 4–10 min for 1T@2H MoS_2 nanostructures, although these materials are generally synthesized rather than directly exfoliated from bulk crystals. Future development should focus on continuous-flow reactors, safer and recyclable intercalants, standardized process reporting, solvent recovery, energy-efficiency assessment, and improved temperature and reagent control during scale-up. Overall, these innovations improve yield and exfoliation efficiency while reducing processing time and potentially energy demand; however, their practical advantages must be evaluated alongside solvent and reagent sustainability, process reproducibility, and scalability to establish truly efficient and environmentally responsible exfoliation routes.

1.5. Electrically Driven Exfoliation

1.5.1. Driving Force and Mechanism:

Electrochemical exfoliation is a top-down production method in which an externally applied electrical potential drives ionic or molecular species into the interlayer spaces of a layered bulk electrode. This insertion weakens the out-of-plane interactions between neighboring sheets and promotes the release of monolayer or few-layer nanosheets [32, 54]. The technique originated from early investigations of graphite intercalation compounds and lithium graphite battery chemistry. Its scope has since expanded beyond graphene to include transition-metal dichalcogenides, black phosphorus, post-transition-metal chalcogenides, MXenes, metal–organic frameworks, and a variety of emerging elemental materials [54, 55]. A typical electrochemical cell consists of the layered precursor as the working electrode, a chemically stable counter electrode, and an aqueous or organic electrolyte. A reference electrode may also be included when accurate control of the applied potential is required [32, 54]. During anodic exfoliation, negatively charged ions such as SO_4^{2-}, HSO_4^-, Cl^-, ClO_4^-, BF_4^-, PF_6^-, and oxalate species migrate into the positively polarized precursor. By contrast, cathodic exfoliation introduces Li^+, Na^+, K^+, or bulky tetraalkylammonium cations into a negatively polarized layered crystal [32, 55]. Charge transfer between the intercalated species and the host lattice reduces the effective van der Waals attraction between the layers. At the same time, solvation, lattice distortion, electrostatic repulsion, and the evolution of gases such as H_2, O_2, SO_2 , or CO_2 generate additional pressure within the interlayer galleries [32, 54, 56]. Anodic exfoliation is generally more rapid because electrochemically generated radicals create openings at crystal edges and grain boundaries. Cathodic processing, however, causes less oxidation and is therefore better suited to semiconductors that are sensitive to oxidation or phase transformation[32, 54]. Alternating-current processing combines repeated anodic activation with cathodic reduction, whereas bipolar electrochemistry polarizes electrically isolated particles between feeder electrodes, allowing powders to be exfoliated without direct wired contact [32, 39, 56].

1.5.2. Scale-Up Evidence and Benchmark Performance

Electrochemical exfoliation provides some of the highest laboratory-scale production rates reported for top-down synthesis of 2D materials. Direct electrochemical processes commonly achieve yields of approximately 30–80%, while graphene production rates can exceed 10 g h^{-1} [39]. Sulfate-mediated anodic exfoliation of graphite has produced predominantly 1–3-layer graphene at 16.3 g h^{-1}. Alternating-current and dual-electrode configurations have reached approximately 20 and more than 25 g h^{-1}, respectively, with monolayer or few-layer fractions often exceeding 70–75% [39, 54, 55].

In radical-controlled ammonium-sulfate exfoliation, the addition of TEMPO maintained a production rate of 15.1 g h^{-1} while decreasing the Raman (I_D/I_G) ratio to approximately 0.1, increasing the C/O ratio to 25.3, and yielding carrier mobilities of approximately 405 cm^2 V^{-1} s^{-1} [39, 54, 55]. Electrochemical exfoliation has also demonstrated high performance for materials other than graphene. Anodic exfoliation of MoS_2 produced sheets 0.9–1.3 nm thick with lateral dimensions of 5–50 µm. Quaternary-ammonium-assisted exfoliation of ReS_2 generated monolayers larger than 20 µm, whereas $NbSe_2$ processes yielded more than 75% monolayers with lateral dimensions approaching 300 µm [57].

Cathodic exfoliation of black phosphorus has achieved yields above 80% and thicknesses of approximately 1.1–3.7 nm. In weak-Lewis-acid systems, the resulting sheets displayed average lateral dimensions of 77.6 ± 15.0 µm.

Electrochemical processing of In_2Se_3 similarly produced an ~83% yield, with an average sheet size of 8.6 μm [32, 57]. Characterization using AFM, HRTEM, Raman spectroscopy, XPS, and electron diffraction generally confirms few-layer morphology and high crystallinity. However, product quality remains highly dependent on electrolyte composition and applied potential [32, 54, 57]. During Li-assisted processing of TMDs, excessive electron injection may convert semiconducting 2H-MoS_2 into metallic 1T or 1T′ phases. Although this transformation improves conductivity and electrochemical activity, it can decrease transistor mobility and switching performance by several orders of magnitude [22, 32]. The principal strength of electrochemical exfoliation is its ability to integrate high throughput, high yield, adjustable product characteristics, and relatively simple instrumentation within a single processing platform [32, 39, 54]. In optimized systems, the electrode expands visibly within seconds or minutes, and complete exfoliation can be achieved in less than one hour. This is considerably faster than solvent-based sonication methods, which may require hundreds of hours to generate concentrated dispersions [31, 54, 57]

Independent regulation of electrical parameters enables control over intercalation depth, reaction rate, layer number, lateral dimensions, defect density, oxidation level, surface functionality, electronic structure, and crystalline phase [32, 54, 56] . The process is also inherently compatible with solution-based manufacturing because exfoliated nanosheets detach directly into the electrolyte. They can subsequently be processed into inks, coatings, composite fillers, freestanding membranes, or printed structures [32, 39, 54].

Compared with prolonged cavitation-assisted exfoliation, electrochemical processing is more effective at preserving large lateral dimensions. This advantage is illustrated by MoS_2 sheets reaching 50 μm, black-phosphorus sheets averaging approximately 77.6 μm, and $NbSe_2$ monolayers approaching 300 μm[57]. Cathodic treatment in organic electrolytes can retain highly crystalline, minimally oxidized semiconductors, whereas anodic and alternating-current systems provide substantially higher production rates when moderate functionalization is acceptable [32, 39, 54].

Electrochemical exfoliation can additionally be integrated with doping, phase engineering, defect generation, functionalization, etching, and composite assembly, reducing the need for several separate post-synthesis steps [32, 54, 57, 58] For example, diazonium-assisted cathodic processing simultaneously exfoliated and functionalized semiconducting 2H-MoS_2, decreased its thickness from approximately 60 to 4 nm, suppressed restacking, and enhanced the measured supercapacitor capacitance by approximately 25% without requiring prior conversion to the metallic 1T phase [58]. The electrochemical scale-up metrics are summarized in Table 4.

Table 4. Comparative scale-up metrics for electrochemical exfoliation production rate, yield, dimensions, and quality.

Method	Production rate	Yield	Thickness / lateral size	Energy / time	Quality notes	Ref
Sulfate-mediated anodic graphite	16.3 $g.h^{-1}$	—	1–3 layers	—	—	[39, 54, 55]
AC / dual-electrode graphene	20–25+ $g.h^{-1}$	Monolayer/few-layer 70–75%	—	—	—	[39, 54, 55]
TEMPO-controlled ammonium sulfate graphene	15.1 $g.h^{-1}$	—	—	—	I-D/I-G ~0.1, C/O 25.3, mobility ~405 $cm^2 V^{-1}s^{-1}$	[39, 54, 55]
Anodic MoS_2	—	—	0.9–1.3 nm thick, 5–50 μm lateral	—	—	[57]
Quaternary-ammonium ReS_2	—	—	Monolayers >20 μm	—	—	[57]
$NbSe_2$ electrochemical	—	>75% monolayer	~300 μm lateral	—	—	[57]
Cathodic black phosphorus	—	>80%	1.1–3.7 nm thick, 77.6±15.0 μm lateral	—	—	[32, 57]
In_2Se_3 electrochemical	—	~83%	Avg. 8.6 μm sheet size	—	—	[57]
Diazonium-assisted cathodic MoS_2	—	—	Thickness 60→4 nm	—	+25% supercapacitor capacitance	[58]

1.5.3. Quality Risks and Failure Mechanisms

Despite its scalability, electrochemical exfoliation involves an inherent compromise between efficient delamination and preservation of the original crystal lattice. In aqueous anodic systems, hydroxyl and oxygen-containing radicals attack crystal edges and grain boundaries, facilitating anion insertion. If radical exposure is not adequately controlled, however, it can cause basal-plane oxidation, vacancy formation, oxygen-containing functional groups, and structural disorder. [32, 54, 56]. Cathodic Li^+ intercalation limits oxidative damage but may introduce sufficient charge to transform semiconducting 2H-TMDs into metallic 1T or 1T′ phases. Such phases are beneficial for catalysis and energy-storage applications but are unsuitable for many transistor and optoelectronic devices. [22, 32]. The metallic 1T phase is also metastable and may return to the thermodynamically preferred 2H phase within weeks, raising significant concerns about long-term phase stability [22]. Traditional direct electrochemical exfoliation depends on continuous electrical contact with a sufficiently conductive precursor. Premature electrode fracture interrupts current flow, restricts deep intercalation, and generates nonuniform mixtures containing both thick fragments and thin nanosheets[32, 39, 55]. Although organic solvents and ionic liquids can suppress oxidation and widen the electrochemical stability window, their use may increase

cost, flammability, toxicity, solvent-recovery requirements, and residual contamination[32, 39, 55]. Additional treatment by sonication, centrifugation, dialysis, annealing, washing, or density-based fractionation may still be necessary. These steps reduce the effective recovery of application-grade material and weaken claims that the technique is genuinely a one-step process [32, 52, 56]. Cross-study comparisons are also complicated by inconsistent definitions of exfoliation yield, limited reporting of batch-to-batch reproducibility, and the inclusion of thick particles or chemically modified products in reported production rates [32, 52, 56].

1.5.4. Recent Innovations and Improvements

Recent investigations have increasingly emphasized electrolyte and reactor engineering to retain the beneficial effects of intercalation while limiting oxidation, fragmentation, and unwanted phase changes. Neutral sulfate salts, including Na_2SO_4, K_2SO_4, and ($(NH_4)_2SO_4$), have replaced concentrated acids in high-rate graphene exfoliation. Radical-scavenging additives such as TEMPO, thiourea, and Co^{2+} can then suppress oxidative damage after the initial opening of graphite edges. [39, 54, 55]. Alternating-current and programmed-potential systems repeatedly reverse electrode polarity, combining rapid anodic activation with cathodic reduction. Dual-electrode cells, meanwhile, generate exfoliated products simultaneously from both electrodes and have achieved graphene production rates above 20–25 g h^{-1}[39, 54, 55]. For phase-sensitive TMDs, bulky quaternary-ammonium ions such as TBA^+, TPA^+, THA^+, and CTA^+ provide substantial steric expansion while donating far fewer electrons than Li^+. This preserves semiconducting phases and enables the production of unusually large nanosheets [32, 54, 57]. Weak-Lewis-acid tetra-n-butylammonium acetate systems suppress hydrogen evolution during black-phosphorus exfoliation, thereby limiting P–P bond damage and producing ultralarge domains. PVP- and diazonium-assisted electrolytes can simultaneously stabilize, functionalize, and prevent the restacking of newly formed TMD sheets [57, 58]. Electrochemical processing has also been extended to MXenes and other chemically complex layered precursors through fluoride-free NH_4Cl/TMAOH electrolytes, concentrated water-in-salt battery electrolytes, molten LiCl/KCl salts, and ionic liquids such as [BMIM][PF_6] [32, 54, 57]. Bipolar electrode configurations overcome the need for direct electrical contact by enabling the exfoliation of suspended particles. Electro-Fenton methods provide another emerging strategy, using electrochemically regenerated hydroxyl radicals to progressively transform MoS_2 sheets into nanoporous structures and quantum dots measuring 3–8 nm [32, 54, 56]. Future progress is likely to involve continuous-flow electrode feeding, recyclable, low-toxicity electrolytes, in situ Raman or XPS monitoring, automated potential regulation, and data-driven process optimization for more reproducible industrial production [32, 54, 57].

1.6. Photon- and Field-Driven Exfoliation

1.6.1. Driving Force and Mechanism:

Laser-assisted exfoliation is a top-down technique that uses concentrated optical energy to weaken or overcome interlayer van der Waals forces in a layered bulk material, generating monolayer or few-layer nanosheets. After the earliest demonstrations of pulsed-laser exfoliation of graphite, the approach was extended to transition-metal dichalcogenides. A notable advance occurred in 2018 with the direct exfoliation of MoS_2, WS_2, $MoSe_2$, and WSe_2 using an 800 nm, 80 fs Ti: sapphire laser [59]. The dominant mechanism is photothermal. Laser photon absorption produces rapid localized heating, out-of-plane lattice expansion, interfacial stress, and deformation sufficient to separate neighboring layers. When short laser pulses are employed, photomechanical pressure and shock-wave generation can further assist delamination [59-61]. In liquid-phase photoexfoliation, laser-induced expansion exposes the layer edges and facilitates penetration of solvent molecules into the interlayer galleries. Local formation of supercritical fluid or bubbles then provides an additional mechanical driving force for exfoliation [62]. Photochemical reactions may occur simultaneously, including chalcogen-vacancy formation, oxidation, bond cleavage, phase conversion, and reactions between the irradiated solid and the surrounding solvent. These processes require careful control to prevent material degradation[60, 61]. Ultrashort femtosecond pulses are especially advantageous because they transfer energy more rapidly than it can dissipate through the lattice, reducing the heat-affected region relative to continuous-wave or nanosecond irradiation [59]. At a more theoretical level, nonlinear-phononic strategies have recently proposed the use of a 300 fs terahertz pulse to selectively disrupt out-of-plane bonds and transform covalently bonded wurtzite BN into layered hBN. Such an approach could potentially extend optical exfoliation to materials that do not initially possess a van der Waals layered structure[63].

1.6.2. Scale-Up Evidence and Benchmark Performance

The thickness, lateral dimensions, and structural quality of laser-exfoliated nanosheets depend strongly on laser wavelength, pulse duration, fluence, repetition rate, irradiation time, solvent environment, and processing atmosphere. Femtosecond irradiation at 800 nm, 1.2 W, and 1 kHz transformed bulk TMDs into approximately 3–4-layer nanosheets within 60 min. The resulting flakes had lateral dimensions of approximately 100–200 nm, while AFM, SEM, Raman spectroscopy, and photoluminescence measurements confirmed their few-layer nature and enhanced optical response [59]. More quantitative yield data were obtained using 248 nm, 8 ns KrF-laser photo exfoliation. This method produced graphene, BN, and MoS_2 at an approximately 30% yield without stirring and an approximately 40% yield when the suspension was stirred at 300 rpm [62]. Increasing the fluence from 1.5 to 4 J cm^{-2} reduced the average lateral dimensions from several hundred nanometers to approximately 20–30 nm, indicating that stronger irradiation promotes thinning but also causes greater lateral fragmentation [62]. Under optimized conditions, the exfoliated graphene showed no prominent

Raman D band and an (I-D/I-G) ratio as high as approximately 2.21. TEM and selected-area electron diffraction further verified that crystalline ordering was retained[62]. Laser-mediated phase processing has achieved optical spot sizes of approximately 1.3 μm and converted regions approximately 2 μm wide. Nitrogen-processed 1T′–2H–1T′ MoS_2 transistors displayed a mobility of approximately 0.6 $cm^2 V^{-1} s^{-1}$ [64]. Related hybrid strategies have also shown precise control. CO_2-laser fragmentation reduced pre-exfoliated BP to sub-100-nm particles [65], whereas blister-based laser transfer deposited approximately 0.3 nm-thick monolayer hBN with transfer probabilities of up to approximately 93% [66]. Although these findings demonstrate considerable positional and thickness control, standardized data on mass yield, production rate, defect density, and layer-number distribution remain unavailable for many laser-processing studies. Laser-assisted exfoliation provides several benefits over traditional mechanical cleavage, extended sonication, chemical intercalation, and high-temperature bottom-up synthesis. Because the technique is non-contact, it avoids contamination from adhesive residues and physical processing tools. Focused energy delivery also allows selected regions of a material to be exfoliated, thinned, patterned, or functionally modified without processing the entire sample[60, 61, 67]. Processing times ranging from seconds to approximately one hour are substantially shorter than the prolonged durations commonly required for sonication-based liquid-phase exfoliation[59, 62]. Ultrafast pulses further limit thermal diffusion and can preserve strong intralayer bonds while preferentially disrupting the weaker interactions between adjacent sheets[59].In liquid media, the resulting nanosheets can be collected, concentrated, redispersed, printed, or deposited by drop-casting, avoiding the complex transfer procedures commonly associated with CVD-grown films[59, 62]. Another important advantage is the ability to integrate exfoliation with defect engineering, phase transformation, heterostructure formation, and surface functionalization within a single processing sequence. This multifunctionality has been demonstrated through sulfur-vacancy-rich 1T/2H MoS_2, graphene-passivated BP, and laser-patterned 1T′–2H MoS_2 structures[60, 64, 65]. Direct laser conversion of solution-coated precursors can also selectively form MoS_2 on graphene while protecting the underlying carbon layer from the severe thermal damage associated with conventional furnace treatment [68]. Laser processing therefore offers a distinctive combination of rapid operation, programmability, localized modification, chemical cleanliness, and compatibility with device fabrication. These photons and field-driven scale-up metrics are summarized in Table 5.

Table 5. Comparative scale-up metrics for photon- and field-driven exfoliation yield, dimensions, and quality.

Method	Yield	Thickness / lateral size	Time/conditions	Quality notes	Ref
Femtosecond laser, TMDs (800 nm, 1.2 W, 1 kHz)	Not reported	3–4 layers, 100–200 nm lateral	60 min	Enhanced photoluminescence	[59]
KrF laser (248 nm, 8 ns), unstirred	~30%	—	—	—	[62]
KrF laser (248 nm, 8 ns), stirred (300 rpm)	~40%	Lateral 20–30 nm at high fluence	Fluence 1.5–4 J cm^{-2}	I_D/I_G up to 2.21; fragmentation above 3–3.5 J cm^{-2}	[62]
Laser phase engineering, MoS_2 (N_2 atmosphere)	Not reported	Spot ~1.3 μm, region ~2 μm	—	Mobility ~0.6 $cm^2 V^{-1}s^{-1}$; 26% thickness loss (N_2) vs. 74% (air)	[64]
CO_2-laser fragmentation, black phosphorus	Not reported	Sub-100 nm particles	—	—	[65]
Blister-based laser transfer, h-BN	Not reported	~0.3 nm thick monolayer	—	Transfer probability up to ~93%	[66]

Abbreviations:TMDs, transition metal dichalcogenides; KrF, krypton fluoride; rpm, revolutions per minute; I_D/I_G, defect-to-graphitic Raman intensity ratio; MoS_2, molybdenum disulfide; N_2, nitrogen; CO_2, carbon dioxide; h-BN, hexagonal boron nitride.

1.6.3. Quality Risks and Failure Mechanisms

A major limitation of laser-assisted exfoliation is the narrow processing window separating insufficient irradiation from destructive exposure. Excessive power, fluence, repetition rate, or treatment duration may lead to in-plane fragmentation, vacancy formation, oxidation, phase transformation, quantum-dot generation, or complete ablation rather than controlled layer separation[59, 60, 62]. In KrF-laser photoexfoliation, fragmentation of MoS_2 became significant above approximately 3 J cm^{-2}, whereas graphene and BN displayed pronounced fragmentation above approximately 3.5 J cm^{-2} [62] . Similarly, extending femtosecond irradiation of TMDs beyond the optimized conditions generated smaller particles, quantum dots, and MoO_x species instead of controlled monolayers[59].

The surrounding atmosphere also has a substantial influence on product quality. Laser-induced phase conversion of MoS_2 in air resulted in approximately 74% thickness loss and increased oxidation, while processing under nitrogen reduced the thickness loss to approximately 26% but did not completely prevent defect formation [64]. Hybrid transfer techniques introduce additional risks. Repeated femtosecond irradiation, for example, can rupture a metallic release layer and contaminate transferred hBN with molten titanium[66].

Scalability remains another challenge because focused laser treatment is often performed serially and point-by-point, increasing processing time with sample area. Femtosecond laser sources, precision optical systems, scanning platforms, and controlled-atmosphere chambers also involve considerable capital and maintenance expenses[60, 61]. In addition, many studies describe laser processing as highly productive or scalable without reporting mass yield, production rate, energy consumption per gram, wafer-scale uniformity, or long-term reproducibility. This lack of standardized data

complicates direct comparison with shear, microwave, electrochemical, and sonication-based exfoliation methods [59, 62].

1.6.4. Process Intensification and Automation

Recent advances have broadened laser exfoliation from a simple photothermal layer-removal technique to a multifunctional, theoretically guided processing platform. Solvent-assisted photo exfoliation now integrates laser-induced lattice expansion, DMF intercalation, high-field charge redistribution, and bubble-mediated separation. DFT calculations indicate that solvent insertion can enlarge the graphite interlayer spacing to approximately 6.68 Å while lowering the exfoliation barrier[62] .

Single-step CO_2-laser processing has also been used to fragment pre-exfoliated BP while simultaneously converting polyimide into conductive laser-induced graphene. During this process, stabilizing P–C and P–O–C interfacial bonds are formed [65]. Blister-based laser-induced forward transfer is another hybrid approach in which nanosecond or femtosecond pulses move previously exfoliated hBN through direct stamping or gas-phase ejection without exposing the nanosheet directly to the laser beam [66].

Reverse phase engineering has enabled selective conversion of semi-metallic 1T′-MoS_2 into a semiconducting 2H channel under nitrogen, creating seamless in-plane metal–semiconductor contacts[64]. Similarly, selective processing with a 1.06 μm fiber laser has converted an ammonium tetrathiomolybdate precursor directly into MoS_2 on graphene, combining synthesis, patterning, and heterojunction formation in a single procedure [68]. At the theoretical frontier, polarized terahertz pulses have been proposed to resonantly excite polar and antipolar phonons and transform three-dimensionally bonded wBN into a layered hBN structure [63].

Machine learning has also been suggested as a means of optimizing laser wavelength, pulse energy, repetition rate, scan speed, atmospheric composition, and Raman response. However, experimentally validated AI-controlled laser exfoliation remains limited. Further progress will require robust datasets, physically informed models, in situ characterization, and closed-loop adjustment of processing parameters [60, 61].

1.7. Applications and Future Outlook

The preceding sections evaluated force-driven, thermochemical, electrically driven, and photon- and field-driven exfoliation against their individual scale-up metrics, compiled in Table 2, Table 3, Table 4, and Table 5, respectively. Because the application landscape of these four families overlaps substantially, we treat their end-use prospects in a single consolidated section rather than repeating them method by method. The organizing principle adopted below is that an exfoliation route becomes industrially relevant not when it produces the largest mass of material, but when the attribute profile of its product layer-number distribution, lateral dimensions, defect density, phase purity, and residual surface chemistry matches the tolerance of the intended application. Table 6 presents a systematic cross-method comparison of these attribute profiles, along with the principal advantages, limitations, and best-matched applications of each family.

1.8. Automation, ML, and Industrial Outlook

The industrial translation of advanced exfoliation requires more than improving the performance of an individual delamination step. A complete manufacturing system must integrate controlled precursor feeding, reactor operation, real-time measurement of critical quality attributes, data-driven decision-making, automatic adjustment of processing variables, downstream separation, and continuous product collection. Bulk precursors, solvents, electrolytes, and additives are processed through mechanical, electrochemical, hydrothermal, microwave, laser, or hybrid exfoliation systems (Fig.1). Critical process variables, including shear rate, pressure, voltage, temperature, flow rate, feed rate, and residence time, determine product attributes such as layer number, thickness, lateral size, defect density, phase purity, and dispersion concentration. In-line Raman, optical, UV–Vis, conductivity, temperature, and particle-size measurements provide real-time data for model-based or AI-assisted feedback control. Automated actuators adjust reactor conditions, while downstream filtration, washing, classification, concentration, and impurity removal produce qualified materials for electronics, energy storage, coatings, composites, catalysis, and sensing applications.

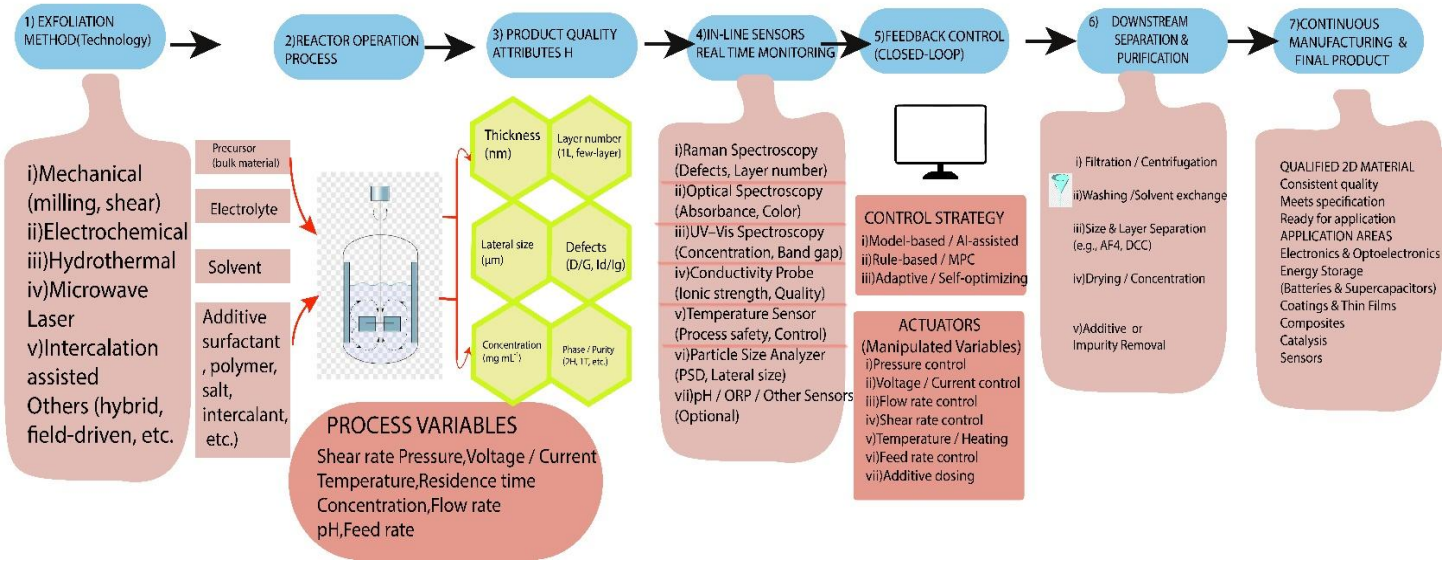

Figure 1: Proposed framework for the transition from advanced exfoliation to reproducible, sensor-integrated, and continuous manufacturing of 2D materials.

1.8.1. Machine Learning-Guided Process Optimization

Optimizing two-dimensional (2D) material production still relies heavily on repeated trial-and-error experiments, even though exfoliation and growth outcomes depend on many interacting chemical, mechanical, thermal, and post-processing factors [21, 22, 69, 70]. In polymer-assisted ball milling, for example, the final product can be influenced by polymer hardness, elasticity, softening temperature, adhesion, friction, and wettability [21] . Robotic mechanical exfoliation introduces another set of variables, including the type of adhesive tape, the number of tape-folding cycles, peeling speed, and the number of transfers [69]. Liquid-phase exfoliation is even more complex because its performance depends on solvent type, surfactant concentration, starting-material concentration, sonication power and duration, shear conditions, and centrifugation speed [22, 70]. Laser and thermal methods are affected by factors such as laser power, scanning speed, pulse properties, reaction temperature, pressure, gas flow, and time-dependent heating conditions [71-73]. Similarly, electrochemical exfoliation depends on electrolyte composition and concentration, applied voltage, current density, intercalating-ion type, and reaction time. However, the reviewed studies have not yet demonstrated direct experimental optimization of these variables using machine learning [70]. Since these parameters often interact in nonlinear ways and may have competing effects on yield, nanosheet thickness, lateral size, defect formation, and production efficiency, changing one variable at a time is unlikely to identify the most favourable processing conditions [22, 70]. Machine learning therefore provides a more systematic way to connect multidimensional processing parameters with measurable quality outcomes, although its practical implementation varies considerably across the available studies [21, 22, 69-75].

In polymer-assisted dry ball milling, machine learning was mainly used to determine how polymer properties affect the morphology of exfoliated h-BN rather than to automatically control milling speed, processing time, or the ball-to-material ratio[21] .The model considered polymer hardness, reduced elastic modulus, softening point, decomposition temperature, adhesion energy, detachment force, friction, and water contact angle. Strongly correlated variables were removed before the model was trained[21] . Several feature-selection methods, including recursive feature addition, recursive feature elimination, exhaustive feature selection, and linear regression, were then used to relate polymer characteristics to nanosheet lateral size, thickness, and aspect ratio [21]. For retaining lateral flake size, the most influential variables were ranked as hardness, adhesion energy, softening point, and friction. Hardness, softening behaviour, and wettability also strongly affected thickness and aspect ratio [21].The results suggested that soft, deformable polymers that can physically grip layered particles may be more effective than polymers selected only for high adhesive strength. This finding challenges the simple assumption that the stickiest polymer will necessarily produce the best exfoliation performance[21] . Experimentally, corn-starch-assisted milling reduced the most commonly observed h-BN thickness from approximately 25 nm without polymer to about 7 nm, while also improving the thickness distribution and aspect ratio[21] . However, the study did not report a machine-learning-specific improvement in mass yield, monolayer percentage, optimization time, or performance compared with a controlled trial-and-error approach. The dataset was also limited to only 17 polymers[21] .

A more direct application of machine learning was demonstrated in robotic mechanical exfoliation combined with Bayesian optimization [69]. The autonomous platform varied adhesive-tape type, the number of tape-folding cycles, peeling velocity, and the number of tape transfers within a search space containing 12,000 possible combinations [69]. Its objective function was based on a composite large-exfoliated-area score that rewarded both the presence and total area of

WSe_2 monolayers larger than 100 μm^2 [69]. Bayesian optimization identified the best-performing conditions after approximately 23 experiments. In comparison, simulated random selection required an average of 485 trials, representing an approximately 21-fold reduction in the number of experiments needed[69] .The model also showed that adhesive-layer thickness and a limited number of folding cycles were more important than the tape's nominal adhesive strength. Excessive folding fragmented the thin crystals and reduced the likelihood of producing large monolayer flakes[69]. The optimized method was later tested experimentally with MoS_2 and graphene, although the main learning process was carried out using WSe_2. Its ability to generalize across a wider range of 2D materials therefore remains uncertain[69] . A related autonomous-growth study used an artificial neural network and adaptive Monte Carlo optimization to generate time-dependent temperature profiles for graphene growth on SiC. This approach increased the monolayer coverage measured by AFM from 22.4% to 88.2%, although it involved thermal growth rather than exfoliation [8].

Evidence supporting machine-learning-guided optimization of laser, electrochemical, and liquid-phase exfoliation is less developed than that available for robotic mechanical exfoliation [22, 70, 72]. A review of laser processing identified laser power, energy density, scanning speed, pulse duration, pulse frequency, spot size, processing path, and in situ Raman or optical signals as possible inputs for machine-learning models [70]. It also described the use of Bayesian optimization with Raman feedback for laser-induced graphene patterning. However, this example involved laser conversion or patterning rather than direct material exfoliation, and it did not report a measurable reduction in defects, improvement in layer-number control, or increased exfoliation yield [72]. In electrochemical exfoliation, electrolyte type and concentration, applied potential, current density, treatment duration, intercalating-ion identity, and cycling conditions have been proposed as useful variables for predicting nanosheet thickness, lateral dimensions, defect concentration, and exfoliation efficiency[70] . Nevertheless, the available discussion was mainly review-based. It did not describe an experimentally validated machine-learning model that selected an electrolyte or operating voltage and then demonstrated improved exfoliation performance [70]. Similarly, a liquid-phase-exfoliation review proposed using supervised learning and interpretable feature-analysis methods to optimize solvent, surfactant, sonication, starting concentration, and centrifugation conditions, but no dedicated model was trained or experimentally validated [22]. By comparison, machine-learning-guided growth has progressed further. In one MoS_2 chemical-vapor-deposition study, a multilayer-perceptron classifier used six growth variables to predict monolayer formation with 75% accuracy and an area under the curve of 0.80 [71].

Overall, most machine-learning models remain limited to laboratory experiments, computational screening, retrospective analysis, or proposed applications rather than being implemented in continuous industrial production [21, 22, 69-75]. The robotic mechanical exfoliation system and the adaptive-Monte-Carlo graphene-growth platform are genuine examples of closed-loop laboratory operation because the conditions proposed by the models were tested experimentally and the characterization results were returned to the optimizer[69, 73] In contrast, the polymer-assisted milling study analysed data from only 17 polymers offline, the MoS_2 layer classifier was based on 130 CVD experiments, and the ZIF-8 study used 90 experimental samples supplemented by 300 virtual samples [21, 71, 76] A separate exfoliation-energy model used a larger dataset containing 4,401 materials labelled through density functional theory and achieved an ensemble-tree R^2 value of 0.89. However, this model predicted intrinsic exfoliation energy rather than processing variables that could be directly controlled during an experiment[74]. These models therefore have limited generalizability. A model trained on h-BN polymer milling, WSe_2 tape exfoliation, graphene growth on SiC, or MoS_2 CVD cannot automatically be expected to perform reliably with different materials, equipment, or exfoliation mechanisms [21, 69, 71, 73]. Even so, machine learning has provided useful scientific insights. It has shown the importance of polymer gripping rather than simple adhesion, adhesive-layer thickness rather than nominal tape strength, bulk decomposition energy in determining theoretical exfoliability, and molybdenum-source temperature in controlling MoS_2 layer formation [21, 69, 71, 74]. These findings are valuable, but small datasets, limited external validation, inconsistent definitions of target outcomes, and the lack of industrial benchmarking prevent strong claims that machine learning has already replaced conventional process-development methods [21, 22, 69-75]

Future progress in machine-learning-guided exfoliation will require well-structured datasets that link complete processing histories with standardized measurements of yield, monolayer fraction, thickness distribution, lateral dimensions, defect density, energy consumption, and production rate [22, 70, 75]. MatSyn25 represents an important step toward building this data infrastructure. It contains 163,240 synthesis and processing records extracted from 85,160 publications, together with more than 1.4 million individual processing parameters [75]. However, databases derived from published literature are still affected by incomplete reporting, inconsistent terminology, differences between equipment, publication bias toward successful experiments, and the limited availability of clearly documented failed conditions[70, 75]. The generation of virtual samples may help address small-data problems. For example, synthetic data improved the R^2 value of a ZIF-8 BET-surface-area prediction model from 0.711 to 0.974 [76]. Nevertheless, artificially generated samples cannot replace sufficiently large, diverse, and experimentally representative datasets. Industrially useful machine-learning systems will also require automated exfoliation equipment, in-line characterization, uncertainty-aware prediction models, traceable process metadata, and closed-loop control algorithms capable of responding to variations between production batches [69, 70, 73]. Cross-material transfer learning and physically informed descriptors will be necessary to determine

whether a model can operate beyond a single polymer–material combination, tape system, reactor design, or 2D compound [21, 69-71, 73, 74]. Machine-learning-guided process optimization is therefore gradually moving from retrospective correlation toward autonomous experimentation. However, its successful transition to scalable industrial exfoliation will depend more on reliable data infrastructure, reproducible characterization, and prospective validation under realistic production conditions than on developing increasingly complex algorithms alone.[69, 70, 73, 75, 76].

1.8.2 Automated Quality Assessment and Classification

Large-scale production of exfoliated 2D materials requires rapid, reproducible, and objective assessment of layer number, lateral size, uniformity, defects, and contamination. Manual optical microscopy is limited by the large number of flakes, operator-dependent interpretation, and variations in illumination, substrates, optics, and imaging systems [25,77–79]. Automated image analysis therefore provides an important route toward standardized quality control. GPU-accelerated platforms combining RGB-based clustering, DBSCAN, Gaussian-mixture modeling, background masking, and parallel processing have achieved approximately 95% pixel-level accuracy while substantially reducing image-processing time, enabling rapid classification of flake thickness, area, and surface coverage across large datasets [25]. Raman spectroscopy provides complementary chemical and structural information, particularly for detecting unexfoliated graphite and sediment in graphene-based materials. Analysis of individual spectra is more sensitive than averaged spectra, although quantitative accuracy remains dependent on sampling strategy and classification methodology [24]. More recently, physics-informed deep-learning models have enabled automated flake detection, layer classification, and thickness estimation across different materials and imaging conditions. Reported accuracies vary among h-BN, graphene, MoS_2, and WTe_2, demonstrating the potential of these approaches while also highlighting the challenges associated with cross-material and cross-instrument generalization [77,78].

Despite these advances, most automated approaches remain laboratory-scale or at-line rather than fully integrated into industrial production [24,25,42,46,77–79]. Microscope configuration, sensor noise, optical artifacts, dataset imbalance, and defects or contaminants not represented during training can affect performance [25,77,78]. Raman-based approaches also require substantial spectral sampling and currently lack universally applicable thresholds or direct integration with exfoliation-process control [24]. A practical industrial system should therefore combine automated optical imaging for high-throughput screening with Raman spectroscopy or other complementary techniques, such as photoluminescence, ellipsometry, or AFM, for ambiguous or high-risk regions. Confidence-based classification could then provide automated pass/fail decisions and feed quality information back to exfoliation or centrifugation processes for real-time parameter adjustment [42,46,79]. Achieving this level of closed-loop quality control will require standardized reference materials, representative datasets containing defects and process failures, cross-instrument calibration, multimodal characterization, reliable uncertainty estimation, and validation under continuous production conditions [42,79].

1.8.3. Continuous-Flow & Industrial Integration

In-line monitoring is increasingly important for scalable 2D-material exfoliation because changes in force, pressure, intercalation, flow, contact conditions, and processing time can alter layer number, flake size, defects, and product uniformity [42,54,80,81]. Conventional techniques such as microscopy, Raman spectroscopy, NMR, LEED, XPS, and ARPES generally characterize materials after processing and therefore provide limited opportunity for real-time process correction [23,42,79–83]. Among these methods, Raman spectroscopy is particularly promising for in-line monitoring because it is rapid, non-destructive, and sensitive to layer number, disorder, strain, and structural changes. In a graphene nanoplatelet production system, fibre-coupled Raman measurements were collected every 10 s, while at-line NMR relaxation provided complementary information on wetted surface area and flake thickness [80]. UHV platforms have also integrated optical imaging with LEED, XPS, and ARPES to evaluate structural, chemical, and electronic properties, although these measurements have largely remained post-process rather than actively controlling exfoliation [23,81–83]. AI-guided approaches have demonstrated feedback-based optimization in graphene growth, but these systems have generally operated between experimental cycles rather than during continuous exfoliation [73]. Thus, a fully autonomous closed-loop exfoliation system has not yet been experimentally established. Future systems should integrate multimodal sensors, real-time data analysis, AI-based decision-making, and automated control of parameters such as pressure, voltage, shear rate, temperature, contact force, and residence time to maintain consistent flake quality and minimize overprocessing or defect formation [42,54,73,80].

1.8.4. Current Limitations of AI-Assisted Exfoliation

These advances, including machine-learning-guided optimization, automated quality assessment, in-line monitoring, and continuous-flow integration, are significant, but they should not be equated with mature autonomous production. A clear distinction remains between offline prediction, automated image classification, model-guided recipe selection, and robotic experimentation and a fully integrated, industrially deployable AI-controlled exfoliation system [42,69,90]. Only a limited number of studies have physically performed exfoliation under AI guidance, and these were validated mainly in single-laboratory settings [69,91,92]. A major barrier is the lack of large, standardized, multi-laboratory datasets. Exfoliation studies vary widely in sonicator geometry, substrate, electrolyte, shear device, reactor configuration, and characterization methods, while key operating parameters are often missing from literature-derived datasets [70,91,93,94]. Most computational datasets focus on DFT-based exfoliation energies rather than experimental outcomes; for example,

the JARVIS-2D benchmark contains only 636 records, insufficient for reliable deep-learning development [74,95–100]. Experimental datasets are similarly limited, including only 960 WSe_2 images for one robotic monolayer detector and benchmark datasets of 6,833 and 517 samples for the physics-informed φ-Adapt framework [69,77]. The scarcity of negative and failed experiments further limits model learning [90,91,94]. Although synthetic-data augmentation has been investigated, MatWheel showed that synthetic samples can introduce distributional bias without consistently improving prediction [98]. Consequently, current ML models largely represent narrow, laboratory-specific experimental snapshots rather than the broader process space required for robust, transferable, and industrially autonomous exfoliation [42,70].

Model limitations compound the dataset problem in ways that make cross-system generalization difficult to achieve. Every ML model reviewed was developed for one material system, one reactor or microscope configuration, one exfoliation mechanism, or one narrow descriptor space [100-102].The cross-property transfer-learning study that explicitly included exfoliation energy as a target demonstrated that the 557-sample dataset was too small and that model performance depended strongly on which source property was used for transfer, with negative transfer occurring on six of nineteen benchmark tasks [96]. The interpretable ML benchmark showed that even with 3,388 filtered exfoliation-energy records, no model achieved a test R^2 above 0.543, and the available compositional descriptors were identified as fundamentally insufficient to represent the physical interactions governing exfoliation [97]. Deep-learning models and AutoML pipelines are broadly acknowledged as black-box systems from which transparent physical mechanisms cannot be extracted [103-105], while post-hoc methods such as SHAP measure statistical feature influence rather than physical causation and can produce explanations that conflict across different models trained on the same data [106]. Models optimized against a single proxy metric whether exfoliation energy, Raman score, photoluminescence intensity, or optical layer classification, do not capture the multidimensional quality space that industrial production requires [69, 73, 92, 107]. The autonomous research system benchmarking study demonstrated that nominal end-to-end automation does not prevent pervasive hallucination, methodological inconsistency, and failure to produce publication-ready outputs, confirming that increased computational expenditure does not guarantee scientific reliability [108].

The deployment gap between AI-assisted prediction and actually operating AI-controlled exfoliation is large and is rarely acknowledged in the literature. Most reported studies are offline predictors, characterization tools, or recipe-selection aids rather than integrated process-control systems [90, 93, 109] Of the exfoliation-relevant studies, only two demonstrated physically connected AI workflows: the robotic mechanical exfoliation platform combined Bayesian optimization with robotic tape folding and monolayer detection [69], and an AI-guided graphene growth study connected an ANN to a cold-wall CVD reactor through a Raman feedback loop [73, 92]. However, the latter concerns growth rather than exfoliation and is cited here as the closest available state-of-the-art comparison. The robotic exfoliation platform identified an optimized condition within 30 trials from a 12,000-combination space, which represents genuine closed-loop experimental optimization [69]. Nevertheless, the system required three desktop robots, custom stamps, specialized software, manual crystal loading, and pre-selected parameter ranges; it did not replenish consumables, recover from faults, or operate unattended for extended periods [69].

The AI-assisted wafer-scale exfoliation review confirms directly that current AI pipelines fall short of a universal and comprehensive framework for predicting, characterizing, and integrating exfoliated and transferred 2D materials [42]. Beyond mechanical exfoliation, no closed-loop AI-controlled system has been reported for liquid-phase, electrochemical, microwave, hydrothermal, or laser-assisted exfoliation [70, 93]. The gap between a published ML model and a production-ready AI-controlled exfoliation reactor therefore remains very large and is rarely stated explicitly in the literature [94, 109, 110]. Experimental validation standards are equally problematic. Reproducibility in ML research is frequently established only at the level of repeatability the same team obtains the same result under identical conditions which provides limited assurance about scientific correctness or cross-condition generalizability [111, 112].

where multimodal data, domain knowledge, dedicated algorithms, and artificial intelligence interact to enable explainable machine learning and accelerate the discovery of next-generation materials (Fig. 2).

Data leakage has been documented as a systemic problem across seventeen scientific fields, and models demonstrating apparently superior performance have been shown to lose their advantage entirely once methodological errors are corrected [113]. The autonomous laboratory that initially claimed a 78% synthesis success rate was shown by independent reanalysis to have achieved approximately 5% genuine novelty, with 42 of 43 claimed successes failing under expert scrutiny [110], demonstrating that an operating robotic system can produce scientifically unreliable conclusions when characterization and phase identification are insufficiently rigorous. For exfoliation specifically, no inter-laboratory reproduction of an AI-guided exfoliation workflow has been reported, no standardized benchmark exists for comparing systems using simultaneously measured yield, monolayer fraction, lateral flake size, defect density, energy consumption, and batch reproducibility [42, 70, 91], and the most direct exfoliation-energy models achieved test errors that left substantial variance unexplained [74, 97]. Human experts remain embedded at every stage of currently reported AI workflows:defining variables, labelling images, setting safety limits, designing objective functions, switching models, interpreting measurements, and validating results [69, 92, 93, 114].The path from AI-assisted to truly autonomous exfoliation requires simultaneously closing dataset, validation, hardware-integration, reproducibility, and scale-up gaps that no single study has yet addressed in combination.Standardized, machine-readable, FAIR-compliant process datasets

including failed and suboptimal experiments must be constructed across laboratories, materials, and equipment platforms [90, 91, 94]. Models must be validated across independent setups rather than only within the generating laboratory, and uncertainty quantification must be integrated so that low confidence predictions trigger human review rather than autonomous action [101, 111, 112]. In-line sensing capable of measuring yield, flake concentration, layer-number distribution, lateral dimensions, defect signals, phase purity, and contamination must be embedded directly in exfoliation hardware rather than applied post-process [42, 70].

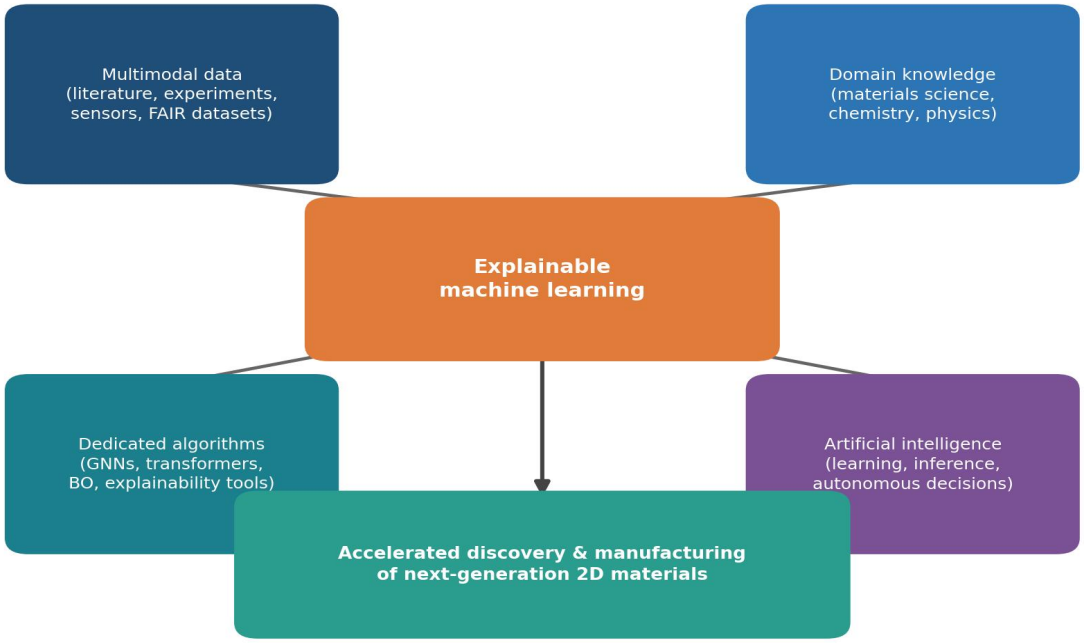

Figure 2. Conceptual framework illustrating the AI-for-materials ecosystem,

Robotic platforms must demonstrate continuous operation including consumable replenishment, fault detection, reactor cleaning, and safety interlocks over durations sufficient to establish long-term reliability [69, 94]. Scale-up from laboratory prototype to pilot plant requires addressing nonlinear heat transfer, mass transport, fluid dynamics, and equipment-specific behaviour that laboratory conditions do not reveal [94]. Techno-economic and life-cycle assessment should accompany scale-up claims so that industrial viability, energy demand, environmental impact, and production cost are evaluated alongside throughput and quality [90]. The available literature does not support a specific timeline for when these requirements will be collectively satisfied. Industrial viability will depend on closing these gaps systematically rather than on developing increasingly sophisticated algorithms applied to the same narrow, laboratory-specific datasets that currently define the field [42, 90, 94, 99, 100].

Table 6 below presents the disaggregated evidentiary basis for these limitations, drawn from the AI-assisted exfoliation studies discussed above. D = Dataset limitation | M = Model limitation | P = Deployment gap (lab vs industrial) | R = Reproducibility issue | B = Broader challenge (cost, expertise, infrastructure).

Table 6. Disaggregated evidentiary basis for AI-assisted exfoliation limitations discussed in Section 7.5.

Ref	Study / Method	AI Tool Used	Dataset Size	Limitation Category*	Specific Limitation Identified	Deployment Status	Experimentally Validated?
[75]	MatSyn25 LLM for 2D material synthesis processes	LLM (MatSyn AI)	163,240 records; 12,317 valid training samples	D + P	Only 12,317 valid samples retained; graphene/hydrothermal overrepresented; hallucination risk; no reactor control	Digital deployment only (web platform)	No
[100]	Small data ML review materials science	Review (no single model)	Most datasets < 1,000 samples	D + M	Fragmented databases; inconsistent standards; models valid only within training domain; generalization unresolved	Proposed only	No
[95]	Mixture of experts for data-scarce materials properties incl. exfoliation energy	Graph neural network + mixture of experts	636 exfoliation-energy samples (JARVIS-2D)	D + M	Only 636 DFT samples; negative transfer in 6/19 tasks; source-task selection unknown; no experimental validation	Computational only	No

Ref	Study / Method	AI Tool Used	Dataset Size	Limitation Category*	Specific Limitation Identified	Deployment Status	Experimentally Validated?
[96]	Cross-property transfer learning exfoliation energy target	ElemNet deep neural network + transfer learning	557 exfoliation-energy samples	D + M	557 DFT-only samples; transfer inferior to scratch model in some cases; composition-only inputs; no physical exfoliation	Proposed only	No
[98]	MatWheel synthetic data for exfoliation-energy prediction	CGCNN + conditional generative model	636 samples (JARVIS-2D); 7% genuine labels	D + M	Synthetic augmentation inconsistent; distribution mismatch; best exfoliation model only marginally improved	Computational only	No
[101]	Computation and ML for materials perspective review	Review (multiple)	N/A — review paper	D + M + P	Inconsistent databases; black-box models; 32 million screened candidates yielded only 18 synthesized materials	Proposed only	No
[110]	Autonomous A-Lab synthesis critical reanalysis	Automated Rietveld refinement + robotic synthesis	58 synthesis targets	M + P	A-Lab claimed 78% success; independent reanalysis found ~5% genuine novelty; AI characterization scientifically unreliable	Physically deployed (lab)	Partial failed
[103]	Interpretable ML for materials comprehensive review	Review (DNN, GNN, LLM, multiscale)	N/A — review paper	D + M + P	Data limited and expensive; black-box models dominate; full-process digital models incomplete; AI-to-AI-driven transition not achieved	Proposed only	No
[104]	Interpretable and explainable ML materials science and chemistry	Review (SHAP, LIME, saliency maps)	N/A — review paper	M	Interpretability ≠ causation; SHAP evaluates impossible feature combinations; shortcut learning; expert judgment still required	Proposed only	No
[102]	Exchange correlation functionals and ML for 2D materials	ML-corrected DFT; graph potentials	N/A — review paper	D + M	PBE-level errors inherited by ML; poor extrapolation outside training domain; no experimental exfoliation validation	Computational only	No
[97]	Interpretable ML for exfoliation-energy and band-gap prediction	XGBoost, TPOT, Roost, SISSO	3,388 exfoliation-energy samples (2DMatPedia)	D + M	Best exfoliation model: test R^2 = 0.543 only; descriptors insufficient; different models identified conflicting important features	Computational only	No
[106]	Interpretable ML for quantum defect host materials — Rashomon set	Random Forest + Gradient Boosting + Rashomon set	~45,000 screened; small labelled training set	M + P	High-accuracy models learned contradictory rules; out-of-distribution predictions unreliable; 110/122 candidates unvalidated	Proposed only (screening tool)	Partial
[99]	ML in materials research decade review and future challenges	Review (matbench, GNNs, DL)	636 samples for matbench_jdft2d (exfoliation energy)	D + M + P	Many problems lack data for deep learning; out-of-distribution generalization unresolved; proprietary models not reproducible	Proposed only	No
[105]	Transformer language models for materials-property prediction	MatBERT transformer + LIME/SHAP/saliency	9,063–55,350 DFT-labelled samples	M + P	Explanation quality: only 49% of LIME, 25% of SHAP explanations reached comprehensiveness > 0.9; no physical exfoliation	Digital (software) only	No
[91]	ML + simulations for scalable 2D-material synthesis (perspective)	Bayesian optimization + ANN + Gaussian process	WS_2: 13 runs; graphene: ~10 runs	D + M + P	Demonstrations single-system only; negative data absent; cross-reactor domain shift unresolved; exfoliation not demonstrated	Lab prototype (growth only)	Partial
[92]	AI-driven autonomous graphene growth ANN + adaptive Monte Carlo	ANN + adaptive Monte Carlo (aMC)	~12 protocols (PTC0–PTC11)	D + M + P	One material, one reactor, one scalar Raman score; human-defined objectives and constraints; no exfoliation; no cross-lab transfer	Lab prototype (growth only)	Yes — growth only

Ref	Study / Method	AI Tool Used	Dataset Size	Limitation Category*	Specific Limitation Identified	Deployment Status	Experimentally Validated?
[94]	Accelerating materials science with autonomous workflows	Active learning + ML + automation (review)	Hundreds to ~2,000 experiments per case	M + P	Revolutionary acceleration not yet realized; most workflows remain expert-mediated; autonomy restricted to narrow sub-tasks	Partially deployed (lab)	Partial
[42]	AI-assisted wafer-scale exfoliation and transfer review	CNN, cGAN, SAC, Bayesian optimization, rheometer	960 images (monolayer detector); ~12,000 BO conditions explored	D + M + P	Current AI pipelines fall short of universal framework; no cross-lab platform; domain shift limits model transfer	Lab prototype	Partial
[90]	Advancing materials discovery through AI review	Review (generative, GNN, LLM, autonomous labs)	N/A — review paper	D + M + P + B	Fragmented datasets; noncovalent interactions poorly represented; proof-of-concept to robust labs far from complete	Proposed (future vision)	No
[113]	Leakage and the reproducibility crisis in ML based science	Logistic regression, Random Forest, AdaBoost	329 papers affected across 17 fields	R + M	Complex models' advantage disappeared after leakage correction; AUC advantage collapsed from 0.14 to 0.01 in case study	N/A	N/A
[108]	MLReplicate benchmarking autonomous research systems	AI Scientist V1/V2, Agent Lab, CycleResearcher	8 ICML papers as benchmark	P + M	No system produced publication-ready outputs; 59% of auto-accepted papers contained fabricated claims; hallucination rate up to 100%	Digital only — ML benchmark	No
[114]	Adaptive AI decision interface electronic material discovery	GPR → Random Forest (adaptive switching)	21 initial + 64 total experiments	D + M + P	No single model adequate throughout campaign; model switching required human decision; one polymer/device/platform only	Lab prototype (OECT)	Yes narrow
[73]	High-throughput optical classification of mechanically exfoliated 2D materials	Mean-shift clustering + DBSCAN + GMM (GPU)	2,916 optical images; ~1–2 examples per class	D + M + P	~95% accuracy but no transfer learning; separate catalog per material-microscope; cannot control exfoliation parameters	Lab software tool	Yes — classification only
[70]	Statistics enabling 2D materials optimization and ML review	DOE, ANN, SVR, Random Forest, Transformer (review)	N/A — review paper	D + M + P + B	Real-time closed-loop control in early stages; datasets overrepresent successful runs; GPU cost prohibitive for smaller labs	Proposed only	No
[69]	Autonomous robotic mechanical exfoliation + Bayesian optimization	YOLO detector + Bayesian optimization (GPR, EI, PI, MI)	960 images; 30 BO trials from 12,000 combinations	D + M + P	Custom hardware; 4 variables only; peeling/transfer angle excluded; no cross-lab transfer; one crystal system (WSe_2 centred)	Lab prototype	Yes — WSe_2 + limited MoS_2/graphene
[93]	Liquid phase exfoliation and electrochemical applications data-driven future	Review — ML proposed for LPE optimization	34 MXene records cited as example	D + M + P	No standardized LPE dataset exists; solvent descriptors unreliable; conflicting literature outcomes; no closed-loop LPE system	Proposed only	No
[77]	phi-Adapt physics-informed domain adaptation for 2D flake analysis	Synthetic pretraining + source-free entropy adaptation (ResNet/ViT)	Real: 6,833 + 517 samples; synthetic: 600,000 images	D + M + P	Graphene accuracy only 47–52% on Uslu benchmark; sensor noise excluded; flake detection AP only 34.1%; no reactor control	Lab software tool	Yes — classification only
[74]	ML prediction of exfoliation energies — data-driven approach	Ensemble trees, SVM, MLR, regression trees	4,401 DFT-computed exfoliation energies	D + M	All labels DFT-derived; poor performance in sparse energy ranges; no experimental exfoliation validation; 150 meV threshold arbitrary	Computational only	No

Ref	Study / Method	AI Tool Used	Dataset Size	Limitation Category*	Specific Limitation Identified	Deployment Status	Experimentally Validated?
[107]	ML-assisted CVD of monolayer h-BN on Fe foil	Gaussian-process regression (3 inputs, 2 outputs)	Limited experimental parameter map; coverage binned 0/0.5/1	D + M + P	Coarse coverage labels; 3 variables only; one material-catalyst-reactor; no autonomous loop; CVD growth not exfoliation	Lab prototype (CVD growth)	Yes h-BN CVD only

Abbreviations: LLM, large language model; AI, artificial intelligence; ML, machine learning; DFT, density functional theory; GNN, graph neural network; DNN, deep neural network; ANN, artificial neural network; CNN, convolutional neural network; SHAP, SHapley additive explanations; LIME, local interpretable model-agnostic explanations; BO, Bayesian optimization; GPR, Gaussian process regression; SVM, support vector machine; CVD, chemical vapor deposition; LPE, liquid-phase exfoliation; R^2, coefficient of determination; AUC, area under the curve; OECT, organic electrochemical transistor.

Conclusion

Recent integration of machine learning, automated experimentation, and in-line characterization demonstrates promising progress toward intelligent manufacturing. Nevertheless, fully autonomous, closed-loop exfoliation remains largely unachieved, with most systems still operating in batch mode and at laboratory scale. The major barriers to industrial translation are therefore not simply improvements in exfoliation efficiency, but the lack of standardized cross-laboratory datasets, reproducible continuous-processing platforms, validated AI-driven process control, and comprehensive techno-economic and life-cycle assessments. Future research should consequently prioritize standardized reporting, continuous and scalable reactor designs, real-time multimodal monitoring, closed-loop AI control, and sustainability-based process evaluation. Addressing these gaps will be essential for transforming advanced exfoliation techniques from laboratory demonstrations into reproducible, cost-effective, and environmentally sustainable manufacturing platforms for next-generation 2D-material technologies.

Acknowledgment

The authors would like to thank Dr. Syed Shoaib Ahmad Shah, Assistant Professor, Department of Chemistry, School of Natural Sciences, National University of Sciences and Technology (NUST), Islamabad, Pakistan, for his valuable guidance and mentorship during the preparation of this manuscript. The literature review and manuscript preparation for this study were conducted at the School of Natural Sciences, NUST, Islamabad, Pakistan.

Author's Contribution

Aoun Muhammad (Conceptualization, literature search and curation, writing original draft, writing review and editing, table and figure preparation, and manuscript revision).

Conflict of Interest: NA.

Funding Resource: This research received no specific grant from any funding agency in the public, commercial, or not-for-profit sectors.

References

1. Twidale, C., & Bourne, J. (2017). What is exfoliation? *Zeitschrift für Geomorphologie*, 267–274.
2. Novoselov, K. S., Geim, A. K., Morozov, S. V., Jiang, D.-E., Zhang, Y., Dubonos, S. V., Grigorieva, I. V., & Firsov, A. A. (2004). Electric field effect in atomically thin carbon films. *Science*, *306*(5696), 666–669.
3. Novoselov, K. S., Jiang, D., Schedin, F., Booth, T., Khotkevich, V., Morozov, S., & Geim, A. K. (2005). Two-dimensional atomic crystals. *Proceedings of the National Academy of Sciences*, *102*(30), 10451–10453.
4. Anasori, B., Lukatskaya, M., & Gogotsi, Y. (2016). 2D metal carbides and nitrides (MXenes) for energy storage, 2017. DOI: https://doi.org/10.1038/natrevmats, 16098.
5. Khazaei, M., Ranjbar, A., Arai, M., Sasaki, T., & Yunoki, S. (2017). Electronic properties and applications of MXenes: A theoretical review. *Journal of Materials Chemistry C*, *5*(10), 2488–2503.
6. Geim, A., & Novoselov, K. (2007). Nat. Mater. *Nat. Mater.*, *6*(3), 183–191.
7. Geim, A. K., & Novoselov, K. S. (2007). The rise of graphene. *Nature Materials*, *6*(3), 183–191.
8. Mannix, A. J., Kiraly, B., Hersam, M. C., & Guisinger, N. P. (2017). Synthesis and chemistry of elemental 2D materials. *Nature Reviews Chemistry*, *1*(2), 0014.
9. Naguib, M., Mochalin, V. N., Barsoum, M. W., & Gogotsi, Y. (2014). 25th anniversary article: MXenes: A new family of two-dimensional materials. *Advanced Materials*, *26*(7), 992–1005.
10. Manzeli, S., Ovchinnikov, D., Pasquier, D., Yazyev, O. V., & Kis, A. (2017). 2D transition metal dichalcogenides. *Nature Reviews Materials*, *2*(8), 1–15.
11. Zheng, W., Tsang, C.-S., Lee, L. Y. S., & Wong, K.-Y. (2019). Two-dimensional metal-organic framework and covalent-organic framework: Synthesis and their energy-related applications. *Materials Today Chemistry*, *12*, 34–60.
12. Cai, J., Han, X., Wang, X., & Meng, X. (2020). Atomic layer deposition of two-dimensional layered materials: Processes, growth mechanisms, and characteristics. *Matter*, *2*(3), 587–630.
13. McFall-Ngai, M., Nyholm, S., & Castillo, M. (2010). Semin Immunol. In: Elsevier.

14. Zhou, D., Gao, Y., Aied, A., Cutlar, L., Igoucheva, O., Newland, B., Alexeeve, V., Greiser, U., Uitto, J., & Wang, W. (2016). J. Controlled Release. In: DOI.
15. Ma, R., & Sasaki, T. (2010). Nanosheets of oxides and hydroxides: Ultimate 2D charge-bearing functional crystallites. *Adv Mater*, *22*(45), 5082–5104. https://doi.org/10.1002/adma.201001722
16. Liu, Y., Qian, J., Liu, H., Deng, J., & Yu, T. (2014). Appl. Biochem. Biotechnol. In: DOI.
17. Wang, Y., Zhang, Q., Deng, H., Shang, L., Chen, D., Li, Y., Zhu, S., & Li, H. (2016). ACS appl. mater. *Interfaces*, *8*(31), 19958.
18. Wang, Z., Yan, X., Hou, Q., Liu, Y., Zeng, X., Kang, Y., Zhao, W., Li, X., Yuan, S., Qiu, R., Uddin, M. H., Wang, R., Xia, Y., Jian, M., Kang, Y., Gao, L., Liang, S., Liu, J. Z., Wang, H., & Zhang, X. (2023). Scalable high yield exfoliation for monolayer nanosheets. *Nature Communications*, *14*(1), 236. https://doi.org/10.1038/s41467–022–35569–8
19. Zhang, C., Tan, J., Pan, Y., Cai, X., Zou, X., Cheng, H.-M., & Liu, B. (2020). Mass production of 2D materials by intermediate-assisted grinding exfoliation. *National Science Review*, *7*(2), 324–332.
20. Nguyen, D. T., Ting, H. A., Su, Y. H., Hofmann, M., & Hsieh, Y. P. (2021). Additive-enhanced exfoliation for high-yield 2D materials production. *Nanomaterials (Basel)*, *11*(3). https://doi.org/10.3390/nano11030601
21. Zhang, J., Zhai, T., Yan, Y., Fang, Q., Liu, Y., Zhu, Y., Tu, W., Lin, C.-Y., Wang, Y., & Lou, J. (2025). Scalable mechanical exfoliation of two-dimensional nanosheets by polymer-assisted dry ball-mill of layered materials and insights from machine learning. *Materials Today Nano*, *30*, 100604.
22. Chavalekvirat, P., Hirunpinyopas, W., Deshsorn, K., Jitapunkul, K., & Iamprasertkun, P. (2024b). Liquid phase exfoliation of 2D materials and its electrochemical applications in the data-driven future. *Precision Chemistry*, *2*(7), 300–329.
23. Sun, Z., Han, X., Cai, Z., Yue, S., Geng, D., Rong, D., Zhao, L., Zhang, Y.-Q., Cheng, P., & Chen, L. (2022). Exfoliation of 2D van der Waals crystals in ultrahigh vacuum for interface engineering. *Science Bulletin*, *67*(13), 1345–1351.
24. Paton, K. R., Despotelis, K., Kumar, N., Turner, P., & Pollard, A. J. (2023). On the use of Raman spectroscopy to characterize mass-produced graphene nanoplatelets. *Beilstein Journal of Nanotechnology*, *14*(1), 509–521.
25. Gasbarro, A., Masuda, Y.-S. D., & Lubecke, V. M. (2025). High-throughput evaluation of mechanical exfoliation using optical classification of two-dimensional materials. *Micromachines*, *16*(10), 1084.
26. Haraguchi, Y., Imai, H., & Oaki, Y. (2022). Selective syntheses of thick and thin nanosheets based on correlation between thickness and lateral-size distribution. *iScience*, *25*(9).
27. Kenaz, R., Ghosh, S., Ramachandran, P., Watanabe, K., Taniguchi, T., Steinberg, H., & Rapaport, R. (2023). Thickness mapping and layer number identification of exfoliated van der Waals materials by Fourier imaging micro-ellipsometry. *ACS Nano*, *17*(10), 9188–9196.
28. Haider, G., Gastaldo, M., Karim, B., Plsek, J., Varade, V., Volochanskyi, O., Vejpravova, J., & Kalbac, M. (2024). Highly efficient bulk-crystal-sized exfoliation of 2D materials under ultrahigh vacuum. *ACS Applied Electronic Materials*, *6*(4), 2301–2308.
29. Cho, Y. J., Sim, Y., Lee, J.-H., Hoang, N. T., & Seong, M.-J. (2023). Size and shape control of CVD-grown monolayer MoS2. *Current Applied Physics*, *45*, 99–104.
30. Akeredolu, B., Ahemen, I., Amah, A., Onojah, A., Shakya, J., Gayathri, H., & Ghosh, A. (2024). Improved liquid phase exfoliation technique for the fabrication of MoS2/graphene heterostructure-based photodetector. *Heliyon*, *10*(3).
31. Coleman, J. N. (2013). Liquid exfoliation of defect-free graphene. *Accounts of Chemical Research*, *46*(1), 14–22.
32. Zhao, M., Casiraghi, C., & Parvez, K. (2024). Electrochemical exfoliation of 2D materials beyond graphene. *Chemical Society Reviews*, *53*(6), 3036–3064.
33. Nguyen, D.-T., Ting, H.-A., Su, Y.-H., Hofmann, M., & Hsieh, Y.-P. (2021). Additive-enhanced exfoliation for high-yield 2D materials production. *Nanomaterials*, *11*(3), 601.
34. Zhang, C., Wu, W., Xian, L., Jiang, B., Liu, F., Lu, K., Huang, J., Zhang, X., Ma, X., & Liu, M. (2025). Universal mild exfoliation of large-size two-dimensional materials for thermal interface composites. *ACS Materials Letters*, *7*(11), 3565–3572.
35. Huang, Y., Sutter, E., Shi, N. N., Zheng, J., Yang, T., Englund, D., Gao, H.-J., & Sutter, P. (2015). Reliable exfoliation of large-area high-quality flakes of graphene and other two-dimensional materials. *ACS Nano*, *9*(11), 10612–10620.
36. Zhao, Z., Lei, W., Zhou, T., Chen, K., Tian, K., Xiong, G., Kuang, S., Xiong, L., Yu, Y., & Huang, L. (2025). Recent advances of two-dimensional molybdenum oxides. *Microstructures*, *5*(2), N/A-N/A.
37. Verma, A., Rani, A., & Yadav, B. C. (2025). Two-dimensional layered metal oxides (2D LMOs) for next-generation electronic devices. *Nanoscale Advances*.
38. Choi, S. H., Yun, S. J., Won, Y. S., Oh, C. S., Kim, S. M., Kim, K. K., & Lee, Y. H. (2022). Large-scale synthesis of graphene and other 2D materials towards industrialization. *Nature Communications*, *13*(1), 1484.

39. Zheng, W., & Lee, L. Y. S. (2022). Beyond sonication: Advanced exfoliation methods for scalable production of 2D materials. *Matter*, *5*(2), 515–545.
40. Li, Y., Kuang, G., Jiao, Z., Yao, L., & Duan, R. (2022). Recent progress on the mechanical exfoliation of 2D transition metal dichalcogenides. *Materials Research Express*, *9*(12), 122001.
41. Huang, X., Han, X., Dai, Y., Xu, X., Zhang, Y., Tian, X., Yuan, Z., Xing, J., Wang, Y., & Huang, Y. (2023). Recent progress in two-dimensional material exfoliation technology and enlightenment for geological sciences. *The Journal of Physical Chemistry Letters*, *14*(45), 10181–10193.
42. Ge, H., Liu, J., Sebek, M., Li, Z., Fu, W., Wang, Z., & Wang, Z. (2025). AI-assisted wafer-scale exfoliation and transfer of 2D materials: Status, challenges and perspectives. *AI for Science*, *1*(1), 013002.
43. Sarmah, A., Morales, M. A., Srivastava, A., Upama, S., Nandi, A., Henry, T. C., Green, M. J., & Vashisth, A. (2023). Interfacial carbon fiber–matrix interactions in thermosetting composites volumetrically cured by electromagnetic fields. *Composites Part A: Applied Science and Manufacturing*, *164*, 107276.
44. Brent, J. R., Savjani, N., Lewis, E. A., Haigh, S. J., Lewis, D. J., & O'Brien, P. (2014). Production of few-layer phosphorene by liquid exfoliation of black phosphorus. *Chemical Communications*, *50*(87), 13338–13341.
45. Pohlman III, W. B. (2018). Graphene based in-plane micro-supercapacitors. In: Google Patents.
46. DiCamillo, K., Krylyuk, S., Shi, W., Davydov, A., & Paranjape, M. (2018). Automated mechanical exfoliation of MoS 2 and MoTe 2 layers for two-dimensional materials applications. *IEEE Transactions on Nanotechnology*, *18*, 144–148.
47. Castellanos-Gomez, A., Buscema, M., Molenaar, R., Singh, V., Janssen, L., Van Der Zant, H. S., & Steele, G. A. (2014). Deterministic transfer of two-dimensional materials by all-dry viscoelastic stamping. *2D Materials*, *1*(1), 011002.
48. Wang, N., Yang, G., Wang, H., Yan, C., Sun, R., & Wong, C.-P. (2019). A universal method for large-yield and high-concentration exfoliation of two-dimensional hexagonal boron nitride nanosheets. *Materials Today*, *27*, 33–42.
49. Wu, P.-R., Liu, Z., & Cheng, Z.-L. (2019). Hydrothermal-assisted shearing exfoliation for few-layered MoS2 nanosheets. *RSC Advances*, *9*(30), 17016–17024.
50. Sharma, K., & Puri, N. K. (2021). Enhanced electrochemical performance of hydrothermally exfoliated hexagonal boron nitride nanosheets for applications in electrochemistry. *Journal of The Electrochemical Society*, *168*(5), 056512.
51. Jiang, H., Li, J., Xie, Y., Du, Y., Zhao, J., Mei, Y., & Xie, D. (2024). Rapid exfoliation and surface hydroxylation of high-quality boron nitride nanosheets enabling waterborne polyurethane with high thermal conductivity and flame retardancy. *Advanced Composites and Hybrid Materials*, *7*(1), 8.
52. Ali, L., Subhan, F., Ayaz, M., Hassan, S. S. U., Byeon, C. C., Kim, J. S., & Bungau, S. (2022). Exfoliation of MoS2 quantum dots: Recent progress and challenges. *Nanomaterials*, *12*(19), 3465.
53. O'Neill, A., Khan, U., & Coleman, J. N. (2012). Preparation of high concentration dispersions of exfoliated MoS2 with increased flake size. *Chemistry of Materials*, *24*(12), 2414–2421.
54. Yang, S., Zhang, P., Shaygan Nia, A., & Feng, X. (2024). Exfoliation and engineering of 2D materials through electrochemistry. *CCS Chemistry*, *6*(10), 2368–2391.
55. Ikram, M., Raza, A., Ali, S., & Ali, S. (2020). Electrochemical exfoliation of 2D advanced carbon derivatives. in *21st Century Advanced Carbon Materials for Engineering Applications-A Comprehensive Handbook*. IntechOpen.
56. Islam, M. A., Serles, P., Kumral, B., Demingos, P. G., Qureshi, T., Meiyazhagan, A., Puthirath, A. B., Abdullah, M. S. B., Faysal, S. R., & Ajayan, P. M. (2022). Exfoliation mechanisms of 2D materials and their applications. *Applied Physics Reviews*, *9*(4).
57. Zhu, D., Zhang, L., Wang, L., Fu, H. Q., Wu, Z., Dong, M., Zou, Y., Lei, Y., Zhang, X., & Zhong, Y. L. (2025). Electrochemical engineering of emerging 2D materials beyond graphene: Progress and prospects. *Small Methods*, *9*(10), 2500197.
58. Zhuo, Y., Kinloch, I. A., & Bissett, M. A. (2023). Simultaneous electrochemical exfoliation and functionalization of 2H-MoS2 for supercapacitor electrodes. *ACS Applied Nano Materials*, *6*(19), 18062–18070.
59. An, S.-J., Kim, Y. H., Lee, C., Park, D. Y., & Jeong, M. S. (2018). Exfoliation of transition metal dichalcogenides by a high-power femtosecond laser. *Scientific Reports*, *8*(1), 12957.
60. Yufei, Y., Chou, L., Gan, Z., Hu, S., & Zeng, X. (2026). Laser processing and functionalization of 2D TMDs materials: A review. *Journal of Alloys and Compounds*, 185986.
61. Vo, T. S., Jeon, B., Hoang, T., Lwin, K. M., Han, S., Vo, T. T. B. C., & Kim, K. (2024). A comprehensive review of laser processing-assisted 2D functional materials and their specific applications. *Materials Today Physics*, *47*, 101536.
62. Kumar, P., Dey, A., Roques, J., Assaud, L., Franger, S., Parida, P., & Biju, V. (2022). Photoexfoliation synthesis of 2D materials. *ACS Materials Letters*, *4*(2), 263–270.
63. Liu, S., Cohen, O., Neufeld, O., & Chen, P. (2025). *Laser driven bulk-to-layered phase transition* [Preprint]. arXiv. https://arxiv.org/abs/2508.04544

64. Zhuravlova, A., Li, M., Alharbi, O., Jeong, Y., Han, B., Gao, L., Bonn, M., Lanza, M., Yang, S., & Ricciardulli, A. G. (2026). Laser-assisted phase engineering of 2D MoS2 for efficient solution-processed electronics. *Advanced Materials*, e23679.
65. Deshmukh, S., Jakobczyk, P., Pyrchla, K., Brzhezinskaya, M., Ficek, M., Yang, B., Yang, N., & Bogdanowicz, R. (2025). Laser-induced heterostructuring of graphene passivated nanoscale black phosphorus frameworks for lithium-ion battery anodes. *Small*, *21*(41), e04480.
66. Goodfriend, N. T., Mirza, I., Bulgakov, A. V., Campbell, E. E., & Bulgakova, N. M. (2025). Laser-induced gas-phase transfer and direct stamping of nanomaterials: Comparison of nanosecond and femtosecond pulses. *Materials Research Express*, *12*(6), 065004.
67. Patra, C., Mondal, S., Mukherjee, R., & Nandakishora, Y. (2025). Advanced synthesis and unique properties of 2D transition metal dichalcogenides for realizing next-generation applications. *ACS Materials Au*, *5*(5), 745–766.
68. Jeon, M. J., Hyeong, S.-K., Jang, H. Y., Mun, J., Kim, T.-W., Bae, S., & Lee, S.-K. (2023). Selective laser-assisted direct synthesis of MoS2 for graphene/MoS2 schottky junction. *Nanomaterials*, *13*(22), 2937.
69. Yang, F., Idehara, W., Tanaka, K., Shinokita, K., Zhao, H., & Matsuda, K. (2025). Autonomous robotic mechanical exfoliation of two-dimensional semiconductors combined with Bayesian optimization. *ACS Nano*, *19*(45), 39005–39013.
70. Abifarin, J. K., & Lu, Y. (2025). Statistics in enabling 2D materials: Optimization, predictive modelling, and data-driven discovery. *Materials Today Physics*, 101814.
71. Lu, M., Ji, H., Chen, Y., Gao, F., Liu, B., Long, P., Deng, C., Wang, Y., & Tao, J. (2024). Machine learning assisted layer-controlled synthesis of MoS2. *Journal of Materials Chemistry C*, *12*(24), 8893–8900.
72. Zhang, X., Zhou, L., Feng, G., Xi, K., Algadi, H., & Dong, M. (2025). Laser technologies in manufacturing functional materials and applications of machine learning-assisted design and fabrication. *Advanced Composites and Hybrid Materials*, *8*(1), 76.
73. Sabattini, L., Coriolano, A., Casert, C., Forti, S., Barnard, E. S., Beltram, F., Pontil, M., Whitelam, S., Coletti, C., & Rossi, A. (2025). Towards AI-driven autonomous growth of 2D materials based on a graphene case study. *Communications Physics*, *8*(1), 180.
74. Wan, Z., & Wang, Q.-D. (2021). Machine learning prediction of the exfoliation energies of two-dimension materials via data-driven approach. *The Journal of Physical Chemistry Letters*, *12*(46), 11470–11475.
75. Li, C., Wang, Y., Wang, Q., Tan, Z., Jia, H., Liu, Y., Qian, L., Ran, N., Liu, J., & Zhang, Z. (2026). Material synthesis 2025 (MatSyn25) data set for 2D materials. *ACS Applied Materials & Interfaces*, *18*(4), 7092–7102.
76. Chen, F., Zhou, H., Yu, X., Zhao, Y., Wang, C., Dai, B., & Han, S. (2025). Dual-stage stacking machine learning method considering virtual sample generation for the prediction of ZIF-8′ BET specific surface area with experimental validation. *Langmuir*, *41*(3), 1733–1744.
77. Nguyen, H.-Q., Nguyen, X. B., Pandey, S., Faltermeier, T., Borys, N., Churchill, H., & Luu, K. (2025). *φ-Adapt: A physics-informed adaptation learning approach to 2D quantum material discovery* [Preprint]. arXiv. https://arxiv.org/abs/2507.05184
78. Nguyen, X.-B., Nguyen, H.-Q., Pandey, S., Faltermeier, T., Borys, N., Churchill, H., & Luu, K. (2026). *QuPAINT: Physics-aware instruction tuning approach to quantum material discovery* [Preprint]. arXiv. https://arxiv.org/abs/2602.17478
79. Lee, Y. C., Chang, S. W., Chen, S. H., Chen, S. L., & Chen, H. L. (2022). Optical inspection of 2D materials: From mechanical exfoliation to wafer-scale growth and beyond. *Advanced Science*, *9*(1), 2102128.
80. Marchesini, S., Glasgow, L., Mackay, J., Visconti, M., Wilhelm, H., Edwards, M., Despotelis, K., Read, O., Casiraghi, C., & Pollard, A. J. (2024). In-process monitoring of graphene nanoplatelet production using Raman spectroscopy and NMR relaxation. *Nanoscale*, *16*(46), 21506–21514.
81. Tallon, B., Lipton-Duffin, J., & MacLeod, J. (2024). Exfoliation of graphene onto Si (111)-7× 7 under ultrahigh vacuum provides some protection against exposure to air. *Langmuir*, *40*(48), 25692–25697.
82. Dan, Z., Sarmasti Emami, R., Feraco, G., Vavali, M., Gerlach, D., Sarott, M. F., Zhu, Y., Rudolf, P., & Grubišić-Čabo, A. (2025). Role of chalcogen atoms in in situ exfoliation of large-area 2D semiconducting transition metal dichalcogenides. *Frontiers in Nanotechnology*, *7*, 1553976.
83. Grubišić-Čabo, A., Michiardi, M., Sanders, C. E., Bianchi, M., Curcio, D., Phuyal, D., Berntsen, M. H., Guo, Q., & Dendzik, M. (2023). In situ exfoliation method of large-area 2D materials. *Advanced Science*, *10*(22), 2301243.
84. Alharbi, T. M., & Raston, C. L. (2023). High conversion continuous flow exfoliation of 2D MoS2. *Nanoscale Advances*, *5*(23), 6405–6409.
85. Kaner, R. B., Nguyen, E. P. N., & Rizvi, S. R. (2022). Continuous production of exfoliated 2D layered materials by compressive flow. In: Google Patents.
86. Wang, Z., Yan, X., Hou, Q., Liu, Y., Zeng, X., Kang, Y., Zhao, W., Li, X., Yuan, S., & Qiu, R. (2023). Scalable high yield exfoliation for monolayer nanosheets. *Nature Communications*, *14*(1), 236.

87. Li, Z., Zheng, F., Qu, K., Ji, N., Tian, W., Zhang, W., Han, X., Zhao, X., Xiao, Z., & Gao, Z. (2026). Scale-up production of high-quality reduced graphene oxide via microwave assistance. *Advanced Functional Materials*, *36*(15), e19920.
88. Kumar, R., Shringi, A. K., Wood, H. J., Asuo, I. M., Oturak, S., Sanchez, D. E., Sharma, T. S. K., Chaurasiya, R., Mishra, A., & Choi, W. M. (2025). Substitutional doping of 2D transition metal dichalcogenides for device applications: Current status, challenges and prospects. *Materials Science and Engineering: R: Reports*, *163*, 100946.
89. Ponce-Torres, A., Rubio-González, A., Montanero, J., Herrada, M., & Galindo-Rosales, F. (2026). *Impulsive hydrodynamic exfoliation into monolayer graphene and nanofragments by transonic flow focusing* [Preprint]. arXiv. https://arxiv.org/abs/2606.17083
90. Otyepka, M., Pykal, M., & Otyepka, M. (2025). Advancing materials discovery through artificial intelligence. *Applied Materials Today*, *47*, 102981.
91. Bonati, L., Novelli, P., & Rossi, A. (2026). From trial-and-error to intelligent workflows: Machine learning and simulations for scalable 2D material synthesis. *2D Materials*, *13*(1), 013001.
92. Sabattini, L., Coriolano, A., Casert, C., Forti, S., Barnard, E. S., Beltram, F., Pontil, M., Whitelam, S., Coletti, C., & Rossi, A. (2024). *Adaptive ai-driven material synthesis: Towards autonomous 2D materials growth* [Preprint]. arXiv. https://arxiv.org/abs/2410.10885
93. Chavalekvirat, P., Hirunpinyopas, W., Deshsorn, K., Jitapunkul, K., & Iamprasertkun, P. (2024a). Liquid phase exfoliation of 2D materials and its electrochemical applications in the data-driven future. *Precision Chemistry*, *2*(7), 300.
94. Andraju, N. (2025). Artificial intelligence in scalable materials synthesis and manufacturing: A comprehensive review.
95. Chang, R., Wang, Y.-X., & Ertekin, E. (2022). Towards overcoming data scarcity in materials science: Unifying models and datasets with a mixture of experts framework. *npj Computational Materials*, *8*(1), 242.
96. Gupta, V., Choudhary, K., Tavazza, F., Campbell, C., Liao, W.-K., Choudhary, A., & Agrawal, A. (2021). Cross-property deep transfer learning framework for enhanced predictive analytics on small materials data. *Nature Communications*, *12*(1), 6595.
97. Dean, J., Scheffler, M., Purcell, T. A., Barabash, S. V., Bhowmik, R., & Bazhirov, T. (2023). Interpretable machine learning for materials design. *Journal of Materials Research*, *38*(20), 4477–4496.
98. Li, W., Chen, Y., Qiu, J., & Wang, X. (2025). *MatWheel: Addressing data scarcity in materials science through synthetic data* [Preprint]. arXiv. https://arxiv.org/abs/2504.09152
99. Jain, A. (2024). Machine learning in materials research: Developments over the last decade and challenges for the future. *Current Opinion in Solid State and Materials Science*, *33*, 101189.
100. Xu, P., Ji, X., Li, M., & Lu, W. (2023). Small data machine learning in materials science. *npj Computational Materials*, *9*(1), 42.
101. Alosious, S., Jiang, M., & Luo, T. (2025). Computation and machine learning for materials: Past, present, and future perspectives: S. alosious et al. *MRS Bulletin*, *50*(10), 1212–1224.
102. Javed, A., Shaheen, M., Shahbaz, M., Ramzan, M. S., Ullah, R., & Jiang, W. (2025). *Exchange-correlation functionals in 2D materials: Applications, challenges, and limitations* [Preprint]. arXiv. https://arxiv.org/abs/2512.00921
103. Jiang, X., Fu, H., Bai, Y., Jiang, L., Zhang, H., Wang, W., Yun, P., He, J., Xue, D., & Lookman, T. (2025). Interpretable machine learning applications: A promising prospect of AI for materials. *Advanced Functional Materials*, *35*(41), 2507734.
104. Korolev, V., & Protsenko, P. (2023). Accurate, interpretable predictions of materials properties within transformer language models. *Patterns*, *4*(10).
105. Oviedo, F., Ferres, J. L., Buonassisi, T., & Butler, K. T. (2022). Interpretable and explainable machine learning for materials science and chemistry. *Accounts of Materials Research*, *3*(6), 597–607.
106. Mahshook, M., & Banerjee, R. (2026). Beyond diamond: Interpretable machine learning reveals design principles for quantum defect host materials. *Physical Review Materials*, *10*(5), 056201.
107. Chaturvedi, P., Naclerio, A. E., Hus, S. M., Vlassiouk, I. V., Lavrik, N., Checa, M., Collins, L., Li, A. P., & Kidambi, P. R. (2026). Sieving hydrogen isotopes via machine learning assisted chemical vapor deposition (CVD) of high-quality monolayer hexagonal boron nitride (h-BN) on iron foils. *Advanced Materials*, *38*(7), e11868.
108. Gaddipati, S. K., Muhammed, D., Keya, F., Rabby, G., & Auer, S. (2026). *MLReplicate: Benchmarking autonomous research systems for machine learning reproducibility* [Preprint]. arXiv. https://arxiv.org/abs/2605.16616
109. Stein, H. S., & Gregoire, J. M. (2019). Progress and prospects for accelerating materials science with automated and autonomous workflows. *Chemical Science*, *10*(42), 9640–9649.

110. Leeman, J., Liu, Y., Stiles, J., Lee, S. B., Bhatt, P., Schoop, L. M., & Palgrave, R. G. (2024). Challenges in high-throughput inorganic materials prediction and autonomous synthesis. *PRX Energy*, *3*(1), 011002.
111. Desai, A., Abdelhamid, M., & Padalkar, N. R. (2025). What is reproducibility in artificial intelligence and machine learning research? *AI Magazine*, *46*(2), e70004.
112. Semmelrock, H., Ross-Hellauer, T., Kopeinik, S., Theiler, D., Haberl, A., Thalmann, S., & Kowald, D. (2025). Reproducibility in machine-learning-based research: Overview, barriers, and drivers. *AI Magazine*, *46*(2), e70002.
113. Kapoor, S., & Narayanan, A. (2022). *Leakage and the reproducibility crisis in ML-based science* [Preprint]. arXiv. https://arxiv.org/abs/2207.07048
114. Dai, Y., Chan, H., Vriza, A., Fan, J., Kim, F., Wang, Y., Liu, W., Shan, N., Xu, J., & Weires, M. (2025). Adaptive AI decision interface for autonomous electronic material discovery. *Nature Chemical Engineering*, *2*(12), 760–770.

Received: July 26th, 2026 **Accepted: August 31st, 2026**